Icarus 225 (2013) 881–897

Contents lists available at SciVerse ScienceDirect

Icarus

journal homepage: www.elsevier.com/locate/icarus

Observations of the northern seasonal polar cap on Mars: I. Spring sublimation activity and processes

C.J. Hansen [a,*], S. Byrne [b], G. Portyankina [c], M. Bourke [a], C. Dundas [d], A. McEwen [b], M. Mellon [e], A. Pommerol [c], N. Thomas [c]

[a] Planetary Science Institute, 1700 E. Fort Lowell, Suite 106, Tucson, AZ 85719, United States
[b] Lunar and Planetary Lab, University of Arizona, Tucson, AZ 85721, United States
[c] University of Bern, Sidlerstr. 5, CH-3012 Bern, Switzerland
[d] USGS, 2255 N. Gemini Dr., Flagstaff, AZ 86001, United States
[e] Southwest Research Institute, 1050 Walnut St., Boulder, CO 80302, United States

ARTICLE INFO

Article history:
Available online 16 October 2012

Keyword:
Mars, Polar caps

ABSTRACT

Spring sublimation of the seasonal CO_2 northern polar cap is a dynamic process in the current Mars climate. Phenomena include dark fans of dune material propelled out onto the seasonal ice layer, polygonal cracks in the seasonal ice, sand flow down slipfaces, and outbreaks of gas and sand around the dune margins. These phenomena are concentrated on the north polar erg that encircles the northern residual polar cap. The Mars Reconnaissance Orbiter has been in orbit for three Mars years, allowing us to observe three northern spring seasons. Activity is consistent with and well described by the Kieffer model of basal sublimation of the seasonal layer of ice applied originally in the southern hemisphere. Three typical weak spots have been identified on the dunes for escape of gas sublimed from the bottom of the seasonal ice layer: the crest of the dune, the interface of the dune with the interdune substrate, and through polygonal cracks in the ice. Pressurized gas flows through these vents and carries out material entrained from the dune. Furrows in the dunes channel gas to outbreak points and may be the northern equivalent of southern radially-organized channels ("araneiform" terrain), albeit not permanent. Properties of the seasonal CO_2 ice layer are derived from timing of seasonal events such as when final sublimation occurs. Modification of dune morphology shows that landscape evolution is occurring on Mars today, driven by seasonal activity associated with sublimation of the seasonal CO_2 polar cap.

1. Introduction

1.1. Background and overview

Every winter ~25% of Mars' CO_2 atmosphere condenses to form a seasonal polar cap (Leighton and Murray, 1966). Northern spring phenomena associated with sublimation of seasonal ice were first imaged at moderately high resolution by the Mars Orbiter Camera (MOC) on the Mars Global Surveyor (MGS) spacecraft (Malin et al., 1998), and Malin and Edgett (2001) noted the appearance of dark spots on the dunes of the north polar erg in the spring. The High Resolution Imaging Science Experiment (HiRISE) on the Mars Reconnaissance Orbiter (MRO) has imaged seasonal activity for three Mars years. This temporal coverage allows us to compare processes extant in one spring to the next, and to compare phenomena in the north to the south. HiRISE's high signal to noise ratio (SNR) facilitates imaging at low light levels (McEwen et al., 2007), which allows imaging of the sublimation process to start just after the Sun rises at latitudes equivalent to Mars' arctic circle. The high SNR is key to getting images of the dark dunes of high enough quality to identify changes when the seasonal frost is gone. The capability of the MRO spacecraft to roll off-nadir enables collection of images in the same location throughout the spring, so we can study the sublimation process as a function of time. This capability also allows us to image features at different emission angles, enabling the acquisition of stereo pairs and production of anaglyphs.

At high northern latitudes dynamic activity associated with sublimation of the seasonal polar cap is mostly found on the dunes. Mars' north polar residual cap is ringed by a vast north polar erg (Cutts et al., 1976; Tsoar et al., 1979), subdivided into 4 sand seas (Lancaster and Greeley, 1990) stretching between ~70N and 85N. Most of the dunes are barchans, barchanoid ridges and transverse dunes, depending on sediment supply, formed by predominantly unidirectional winds (Hayward et al., 2008). The north polar erg has a double ring of wind circulation patterns, divided at approximately 80N, determined from slipface orientation, which show that winds north of 80N blow predominantly from the east and south of 80N blow predominantly from the west (Tsoar et al.,

* Corresponding author.
E-mail address: cjhansen@psi.edu (C.J. Hansen).

0019-1035/$ - see front matter © 2012 Elsevier Inc. All rights reserved.
http://dx.doi.org/10.1016/j.icarus.2012.09.024

1979; Ward and Doyle, 1983; Coleman and Hayward, 2011), at least during the summer and fall when the dunes are free of their protective layer of seasonal ice. The spacing of the dunes varies from sparse to complete coverage. The average dune height is 20–25 m (Garvin et al., 1999) although barchans in less-dense areas average closer to 50 m in height (Bourke et al., 2006). The source of the dark basaltic and gypsum sand in the dunes appears to be the basal unit of the polar layered deposits, the Planum Boreum cavi unit (Byrne and Murray, 2002; Tanaka and Hayward, 2008) and the Upper Polar Layered deposits (Massé et al., 2010, 2012).

In the well-studied southern polar region of Mars seasonal CO_2 ice is at times impermeable and translucent, allowing sunlight to penetrate and warm the ground below (Kieffer, 2000; Langevin et al., 2007). The ice layer sublimates from the bottom, trapping gas between the ice and the surface (Kieffer et al., 2006; Pilorget et al., 2011). This pressurized gas ruptures the ice and escapes, entraining fine material eroded from the surface, carving uniquely martian radially-organized channels in the surface, dubbed "araneiform" (spider-like) terrain (Piqueux et al., 2003; Kieffer, 2007; Piqueux and Christensen, 2008; Hansen et al., 2010; Portyankina et al., 2010). Surface material is transported by the escaping gas to the top of the ice, then deposited in relatively dark fans directed by prevailing winds and slopes (Malin and Edgett, 2001; Thomas et al., 2010). After the ice is gone the fans blend back into the surface. When conditions are favorable fans of bright CO_2 frost, from gas that cools adiabatically after escaping from the subsurface, can form (Titus et al., 2007). We refer to the entire process as the "Kieffer Model."

Southern and northern winters are not identical due to Mars' elliptical orbit, and it is not necessarily the case that processes operating in one hemisphere will be active in the other. Southern winters are longer allowing more CO_2 to condense. Viking, MGS, Odyssey and Mars Express observations show that in the northern hemisphere H_2O atmospheric transport is greater than in the southern hemisphere (Farmer and Doms, 1979; Kieffer and Titus, 2001; Wagstaff et al., 2008; Appere et al., 2011). Observations by MRO of the composition of the seasonal ice cap are discussed in the companion paper by Pommerol et al. (2013).

In this paper we use the terms "frost" and "ice" somewhat interchangeably, but always in reference to the seasonally condensed volatile. MGS gravimetric data combined with MOLA data show that a layer of condensed $CO_2 \sim 1$ m deep (depth is latitude-dependent) initially (Aharonson et al., 2004) gradually compacts to higher density (Matsuo and Heki, 2009).

Piqueux and Christensen (2008) analyzed northern MOC images and proposed the application of the Kieffer model to northern terrain based on MGS data. Slab ice is consistent with MGS Thermal Emission Spectrometer (TES) data (Titus et al., 2001). With dark dunes below a layer of translucent ice the conditions are set up for basal sublimation. When the ice ruptures the gas will escape, carrying sand and dust from the surface of the dune to the top of the seasonal ice layer. Polygonal cracks visible in MOC and HiRISE images are consistent with slab ice cracking from the pressure of the gas confined below and releasing dust and sand-laden gas (Piqueux and Christensen, 2008; Portyankina et al., 2011).

Morphological changes were observed on the dunes (new alcoves and debris aprons) in the second Mars year of HiRISE operation, detected when ice-free images were compared between the two years. Temporal coverage of the same location throughout spring showed that changes in dune morphology could be correlated with seasonal activity (Hansen et al., 2011), and destabilization of the dune brink by gas flow from basal sublimation was proposed as the cause, described further in Section 3 of this paper. The formation of large new alcoves may be initiated by fluidization of eolian sediment from CO_2 sublimation and destabilization of nearby material, provided the CO_2 is blanketed by a layer of sediment (Cedillo-Flores et al., 2011). A purely wind-driven origin has also been proposed (Horgan and Bell, 2012); however, in the southern hemisphere we know new gullies are formed while CO_2 is on the ground, not when the sand is active from the wind (Diniega et al., 2010).

1.2. Investigation goals and data

In this paper we focus on seasonal processes in the northern hemisphere. The questions we want to address with HiRISE data are as follows: What is the nature of the activity associated with sublimation of the seasonal polar cap in the north? Does the northern seasonal polar cap exhibit the same sorts of phenomena as the south? What phenomena are unique to the sublimation of the north seasonal cap? In the first spring observed our emphasis was to characterize the types of seasonal activity extant in northern spring. With images from the second Mars year we identified morphological changes on the dunes of the north polar erg, including new alcoves and debris aprons, caused by seasonal processes. In this third year we are systematically investigating the factors influencing the efficacy of seasonal activity such as slipface orientation and dune morphology and we are monitoring the northern dunes through the current northern summer.

Section 2 describes the variety of activity observed by HiRISE. Section 3 evaluates the processes that are responsible for the observed activity and discusses the applicability of the Kieffer model to the northern hemisphere. Section 4 concludes with north–south comparisons.

The sand dunes in the north polar erg host a wide variety of seasonal phenomena, while there is very little observable seasonal activity in non-dune areas (Kieffer and Titus, 2001). The small HiRISE image size (typically 6 km × 12 km) means that spatial coverage is limited. Only a few sites can be selected for in-depth investigation, which in the context of seasonal processes equates to temporal coverage. Sites that were selected in the northern polar region, primarily on the north polar erg, for detailed study are listed in Table 1 with locations shown in Fig. 1. In order to investigate factors influencing the seasonal sublimation process in our study year 3 we targeted slipfaces facing ~ east and slipfaces facing ~ west, good longitudinal coverage, sites with scarce sand and scattered barchans, transverse dunes at sites with abundant sand, and a variety of dune forms.

Image identifiers starting with "PSP" (Primary Science Phase) are from the first Mars year of MRO's mission, those starting with "ESP_01nnn_mmmm" (Extended Science Phase; 01nnn is the orbit number) are from the second Mars year, and those starting with "ESP_02nnn_mmmm" are from MRO's third Mars year; conventionally labeled MY29, MY30 and MY31, respectively (Clancy et al., 2000). Image series were started at a much earlier L_s in the third Mars year compared to the first and second.

All images unless otherwise noted are the HiRISE RGB.NOMAP product, produced routinely by the HiRISE ground processing pipeline. "NOMAP" signifies that these images are not map-projected. This means that south is up and illumination is from the upper right.

RGB.NOMAP images are calibrated however no pointing or geometric corrections are applied, and they retain full spatial resolution because the pixels are not re-sampled. HiRISE's three monochromatic bands are referred to as "RED", "Blue-Green (BG)" and "InfraRed (IR)" – the IR data is not used in this product. The RGB false-color image is produced using only the RED and BG data. The synthetic blue is generated by multiplying the BG image by 2 minus 30% of the RED image DN for each corresponding pixel (McEwen et al., 2010; Delamere et al., 2010). Each color filter is stretched individually to maximize contrast and stretches are not

Table 1
Sites imaged systematically by HiRISE in study year 3 (MY31) of seasonal campaign. The names are informal, some based on the sand dunes in the science fiction book "Dune."

Latitude	Longitude east	Informal name	L_s imaged year 3	Slipface orientation	Comment
72.29	311.75	South Beach	338, 347, 22, 30, 32, 50, 52, 67, 74	South, southeast	Barchanoid ridges, furrows
73.35	355.1	Windy City	337, 346, 8, 21, 29, 44, 49, 63, 73	East	Scattered barchans
73.65	328.2	Caladan	8, 31, 37, 68	Southeast	Isolated barchans and domes, furrows
73.89	334.7	T-Party	344, 350, 6, 17, 22, 35, 40, 52, 67, 74	South, southeast	T-shaped dunes, domes
74.0	288.3	Erg outlier	10, 23, 36, 50	Northeast	Linear dunes
75.0	300.0	Translucent Ice	336, 346, 16, 22, 29, 34, 39, 42, 49, 54, 66, 76	East, southeast	Linear dunes
75.38	317.36	Variable packing	342, 351, 7, 23, 28, 48	South, southeast	Barchans
75.53	281.87	Ts and Vs	341, 347, 17, 23, 32, 43, 55, 67	Southeast	T- and V-shaped
75.8	94.06	Classic barchan	339, 7, 13, 20, 31, 43, 48, 75, 79	East, northeast	Scattered barchans
76.6	104.1	Romo	14, 21, 39, 61	East, northeast	Barchans
76.63	89.49	Windy City 2	347, 15, 30, 41, 50, 62, 65	Northeast	Barchanoid ridges
76.85	30.24	Chusuk	9, 22, 40, 45, 67, 76	West, northwest	Rounded barchanoid ridges
78.0	84.0	Hagal	14, 20, 30, 55, 64	Southeast	Linear, rounded
80.0	122.5	Arrakis	8, 18, 23, 36, 39, 46, 53, 61, 72, 78, 82	East	Barchanoid ridge
80.0	240.0	Gypsum Source	6, 32, 56, 73	Southeast	Linear, rounded transverse
80.22	217.08	Cool Fans	1, 14, 20, 37, 57, 71, 76	South	Complex
81.0	156.0	Zanovar	0, 35, 49, 69, 73	Northwest	Transverse
81.65	178.8	Gypsum dunes	13, 21, 34, 54, 66, 73	West, northwest	Transverse
83.5	118.5	Tleilax	13, 25, 34, 39, 47, 54, 66, 74, 80	West, southwest	Transverse
84.0	233.2	Buzzel	11, 14, 24, 34, 40, 50, 55, 64, 81	West (but broad distribution)	Barchanoid ridges
84.7	0.7	Kolhar	3, 8, 16, 24, 37, 44, 49, 61, 71, 75	Northwest, north	Barchanoid ridges

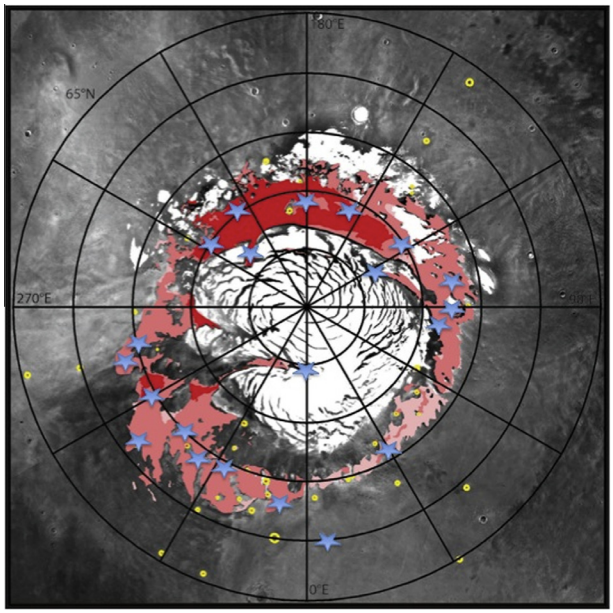

Fig. 1. This basemap of Mars' north polar region was provided by R. Hayward. Yellow circles show craters with dunes. Dark red areas show regions of the polar erg with abundant sand, with dunes almost entirely covering the substrate; pink areas feature sparse coverage by crescentic dunes; the reddish-pink color has a high density of dunes but not complete coverage of the interdune substrate (Hayward et al., 2010). Blue stars indicate the approximate locations of HiRISE study sites. (For interpretation of the references to color in this figure legend, the reader is referred to the web version of this article.)

the same from image to image. Even if stretches were the same colors would vary with atmospheric conditions. Color images are very useful for identifying frost, which is brighter and bluer than bare ground. The contrast between the seasonal ice and surface material on top of the seasonal ice is easy to discern in color images. CO_2 vs. water ice cannot be differentiated in a HiRISE image – for that CRISM data is required, as discussed in the companion paper by Pommerol et al. (2013).

Figs. 2–5 illustrate the full range of HiRISE spatial resolution and coverage: Fig. 2 shows the 1.3 km wide color strip imbedded in the 6.5 km wide image. Fig. 3 zooms into show just the color strip. Fig. 4 zooms in more to a sub-image of the color strip. Fig. 5 is zoomed into almost full resolution.

1.3. Depth of seasonal ice

Mars Orbiter Laser Altimeter (MOLA) and Gamma Ray Spectrometer (GRS) data have been used to calculate the amount of accumulated CO_2 ice in winter as a function of L_s and latitude (Smith et al., 2001; Boynton et al., 2003; Aharonson et al., 2004; Kelly et al., 2006; Litvak et al., 2007), where L_s is the solar longitude, measured from Mars' vernal equinox [$L_s = 0$ is the first day of spring in the northern hemisphere; $L_s = 90$ is the first day of summer]. Values in these papers are generally given as the observed column density in gm/cm^2, because the ice bulk density is not directly measured. The global/temporal average bulk CO_2 density was estimated from MOLA and GRS data to be 500 kg/m^3 (Aharonson et al., 2004). MGS gravimetric data combined with MOLA data show that density increases over the course of a martian winter/spring, varying in the north from 100 kg/m^3 at the beginning of deposition, like light fresh snow or frost, gradually compacting to up to as high as ~1500 kg/m^3, the density of nonporous CO_2 ice, at L_s 60 (Matsuo and Heki, 2009).

Table 2 gives the approximate depth of the CO_2 layer for two latitudes and three times based on the column density derived from Odyssey GRS data (Kelly et al., 2006) and bulk ice density derived from MOLA plus MGS gravimetric data, with a linear increase in density as a function of time (Matsuo and Heki, 2009). (It is helpful to keep these approximate depths in mind when analyzing image data, but it is also important to recognize that these are very coarse estimates – for example interannual variability is completely ignored as are a variety of other factors.)

2. Northern seasonal cap spring sublimation phenomena

This section will serve as both a review and an update with new images from the third northern spring that HiRISE has imaged. HiRISE results have been published in an assortment of papers and abstracts, but not as a comprehensive description of the seasonal processes extant in the northern hemisphere.

2.1. Fans on sand dunes

We use the term "spring activity" to generically describe features that show up on the dunes in the presence of the seasonal layer of frost, and then disappear when the dunes are ice-free.

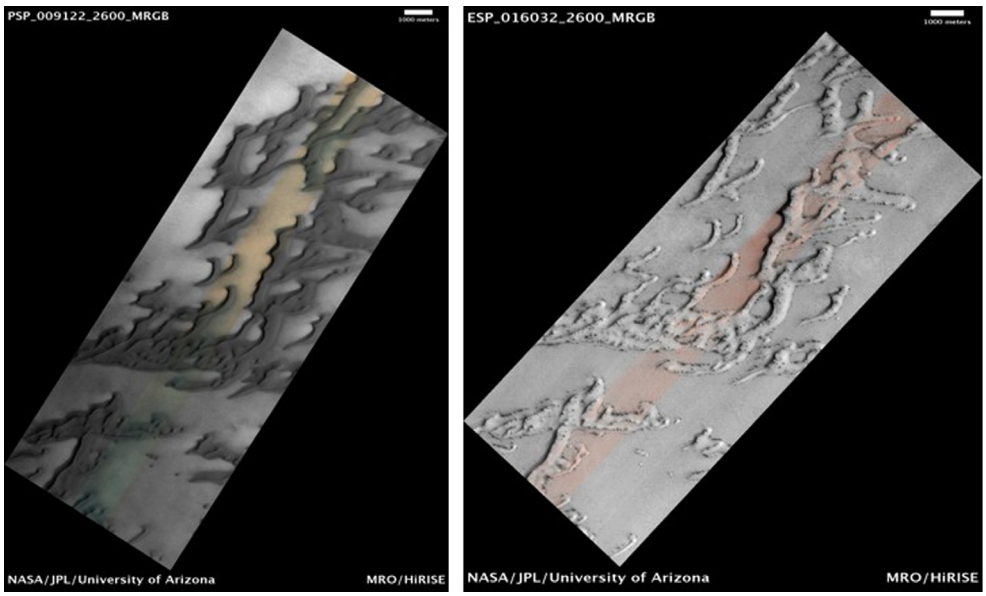

Fig. 2. (a) Map-projected image PSP_009122_2600 on the left, acquired at 80.0N/122.5E, L_s 95.4, shows a region with ice-free barchanoid dunes on a patterned ground interdune substrate. The dark dunes have a surface reflectance of 0.16; the interdune substrate is only slightly brighter (see companion paper by Portyankina et al., 2013). These two images show the full 6.5 km width of the HiRISE images. Color is available only in the ~1.3 km wide center strip. (b) Map-projected image ESP_016032_2600 on the right, taken the following spring at L_s = 29.7, shows seasonal activity concentrated on the dunes. At this latitude and L_s seasonal ice covers the entire scene, ~0.5 m deep, depending on the assumed ice density. These dunes are informally referred to as "Arrakis." (For interpretation of the references to color in this figure legend, the reader is referred to the web version of this article.)

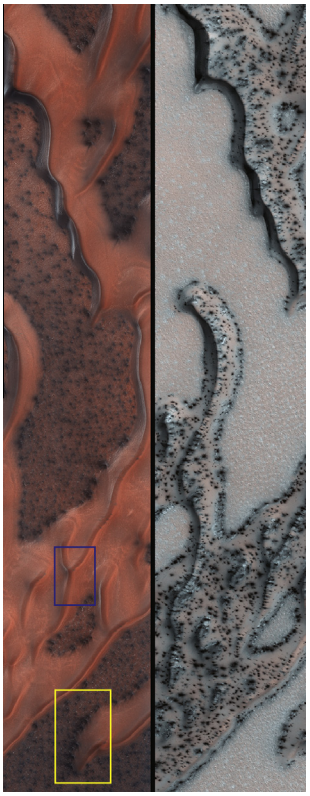

Fig. 3. The image on the left is ESP_024247_2600, acquired at L_s 7.5, at 80N/122.5E. Fans are visible on the interdune substrate but not on the dunes. PSP_007725_2600, the image on the right, was acquired at L_s 47.5, still covered with seasonal ice, with sublimation activity concentrated on the dunes. Both images are ~1.3 km wide. The blue rectangle shows the location of Fig. 5 (and center of Fig. 4); the yellow rectangle shows the location of Fig. 10a.

Fig. 2a and b show a region of dark barchanoid dunes on a relatively brighter interdune substrate without and with seasonal frost cover, respectively. In the spring many small dark fans of fine material are seen deposited on top of the brighter seasonal layer of ice (Fig. 3). This material is being transported from below the seasonal ice layer to the top, in a process that is likely analogous to the well-modeled process that occurs in the southern hemisphere, described briefly above, and discussed in detail in Section 3. Material emerging from below the ice is carried downwind and/or downslope. When the ice is gone the fans are no longer visible, blending back into their source material.

Fig. 3 zooms into the center of this region, dubbed "Arrakis" also imaged by MOC (Kieffer, 2007, Fig. 2). Seasonal activity starts very early at L_s 7.5, first on the interdune substrate, then on the dunes. Fans observed very early on the substrate disappear quickly. If the Kieffer model of basal sublimation is correct this early release of gas may fracture the seasonal ice layer enough on the substrate that fans do not recur throughout spring, because the gas is no longer trapped at all.

A full spring sequence from study year 3 (MY31) is illustrated in Fig. 4 for the Y-shaped dune shown in Fig. 3 (the center of the Y is indicated by the purple box). Between L_s 7 (left side of Fig. 3) and L_s 18 (Fig. 4) spring activity on the dunes has started. Polygonal cracks have opened releasing dune material to be blown downwind in narrow fans. At L_s 39 material propelled from below the seasonal ice layer to the top has been blown in a number of directions and also slides downslope. The dune margin is a source of material to be blown downwind, obvious at L_s 46. By L_s 72 patches at the top of the dunes are bare of seasonal ice.

The images shown in Fig. 5a–c are sub-images of pictures taken throughout spring in MY30 at the same location in Arrakis as Figs. 2 and 3, zooming into the blue box indicated in Fig. 3. Many small relatively dark fans of fine material are seen deposited on top of the brighter seasonal layer of ice. Fig. 5b, taken at L_s 46.8, shows bright fans emanating from the same sources as the dark fans. Analogous to the southern hemisphere, this shows that when atmospheric conditions are favorable fans of bright frost, CO_2 that cools adiabatically after escaping from the subsurface, may form (Titus et al., 2007). Piqueux and Christensen (2008) reported that they had not found bright fans in MOC images in the north polar

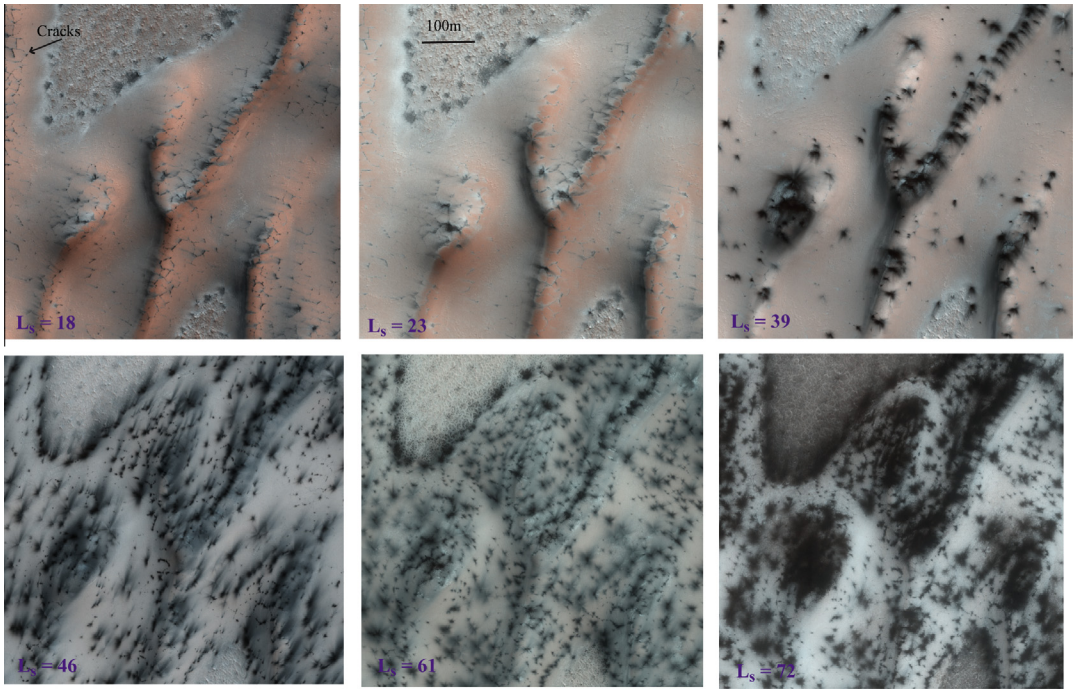

Fig. 4. The sequence of spring activity is illustrated for Arrakis, using the following images, from left to right: (top) ESP_024537_2600, ESP_024669_2600, ESP_025104_2600, (bottom) ESP_025315_2600, ESP_025737_2600, ESP_026080_2600. An estimate of ice thickness at L_s 18 is 60 cm; estimated thickness at L_s 46.1 is ~25 cm.

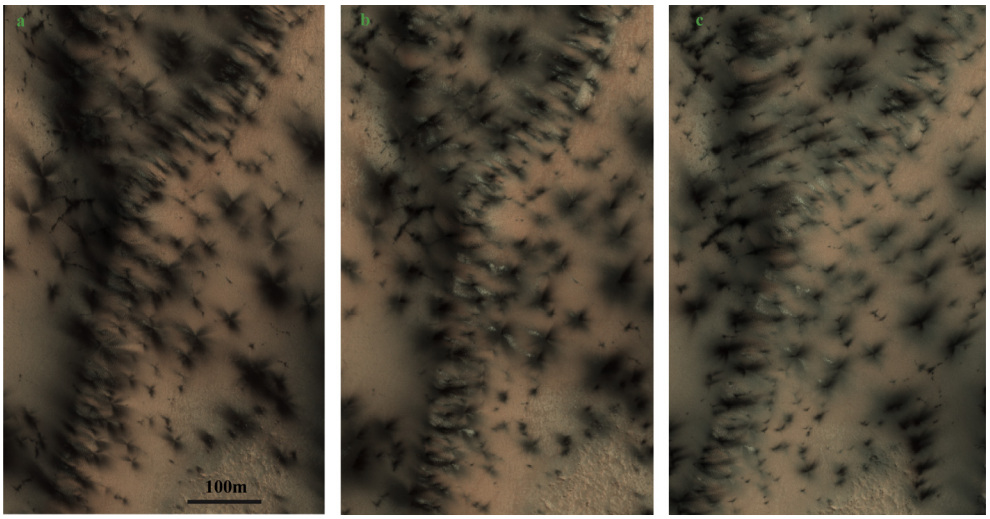

Fig. 5. (a) Zooming in on the center of the Y-shaped dune in this scene, a sub-image of ESP_016388_2600 acquired at 80N/122.5E, L_s 42.2, fans of dark dune sediment can be seen on top of brighter seasonal ice. The direction of fans is downslope and/or directed by the wind. (b) Bright fans also form when the conditions are right, as shown in this sub-image of ESP_016520_2600, L_s 46.8. (c) Dark fans are fading as material sinks into the ice in this sub-image of ESP_016612_2600, acquired at L_s 50.0.

region; however, this may be due to their small scale or MOC's limited temporal coverage. The bright fans on these dunes were observed at L_s 46.8. No bright fans were observed at L_s 42.2, and only the remnants of those at 46.8 are visible at L_s 50.0.

In the southern hemisphere, for example, in the region known informally as Ithaca, at 85.13S/180.67E, bright fans were only observed at L_s 187. At $L_s < 185$ and $L_s > 211$ there were no visible bright fans. A different mechanism for producing bright fans was suggested by Pommerol et al. (2011) based on the analysis of successive HiRISE images acquired in Ithaca. In Ithaca, around L_s 200, the external edges of the largest dark fans suddenly brightened significantly and show a pronounced blue color in false-color images ("blue haloes"). Smaller dark fans can even become entirely bright at this time. For the largest fans, the blue color rapidly disappears while smaller fans might remain hidden for a much longer time, possibly until the end of spring. Sinking of dark sand grains through the ice layer or formation of micro-dimples around each deposited mineral grain (Kieffer, 2007) could explain the observed evolution. Dark grains deposited at the surface of clean and compact CO_2 ice will absorb the sunlight very efficiently, warm-up, and sublime the CO_2 ice around them. The hole carved by the grain may remain open (micro-dimples) or be sealed by re-condensation of the CO_2 on top of the grain (sinking). The "cleaned" surface previously covered by the dark fan can thus appear brighter (and bluer) than the surrounding ice, producing bright fans at the exact location where the dark fans were.

Table 2
The depth of the CO_2 layer is computed from column densities determined from GRS data* (Kelly et al., 2006) with a linearly increasing density** (Matsuo and Heki, 2009) to provide a convenient estimate when looking at the images. Depths will vary from year-to year, and where on the dune (slipface vs. stoss) the frost was deposited.

Latitude	Column density* (g/cm^2)	CO_2 layer density** (g/cm^3)	Depth (cm)
L_s = 350		0.56	
75	45		80
82.5	65		120
L_s = 20		0.86	
75	34		40
82.5	60		70
L_s = 50		1.15	
75	10		9
82.5	35		30

Fig. 5 shows evidence for both processes occurring in the northern hemisphere with similar effects on the temporal evolution of the appearance of fan deposits. The small bright fans not associated with previous dark fans (5b) may be fresh deposits of frost, while the gray appearance of fans in false color images may be due to the change in contrast of the originally dark fans. In the case illustrated in Fig. 5 comparison of dark fans in Fig. 5a–c shows that the sinking of material into the ice layer and/or the development of micro-dimples around the mineral grains may cause the gray appearance where there was a dark fan. In addition to the processes already described, the final fading of the dark fans might be explained by another process described for southern polar areas by Kieffer (2007). If the dark mineral material actually consists of aggregates of smaller particles the disaggregation of these agglomerates can explain the progressive brightening of the dark deposits.

Barchan dunes have a distinctive sequence of seasonal activity, as shown in Fig. 6, a more southerly site at the edge of the polar erg. Activity begins at the interface of the substrate with the dunes where dark sand is observed in fan-shaped deposits, presumably propelled out from under the seasonal ice layer. On the flatter stoss side of the dune polygonal cracks develop (Piqueux and Christensen, 2008; Portyankina et al., 2011). At L_s 7 dark material emerges from the cracks; by L_s 13 the contrast of the fans is observed to fade, as the material (possibly) sinks back into the ice. Bright frost can be seen condensing around the cracks at L_s 20. Bright fans may emerge, as shown at L_s 43. At the end of the spring sequence, L_s 79, ice lingers in cold traps, then disappears.

A similar sequence takes place at the more northerly "Kolhar" site although some types of activity occur later, as shown in Fig. 7. For example polygonal cracks show up at L_s 24, and bright fans at L_s 61.

A typical sequence of defrosting for dunes in an area with abundant sand covering most of the substrate is shown in Fig. 8. This series at 80.22N/217.1E begins at L_s 1 before seasonal activity has started. By L_s 14 fans of sediment have emerged along the dune crest and thin polygonal cracks can be detected (narrow lineations – these are easier to see in Fig. 11c, a different sub-image of the same site at L_s 14). Non-fan-shaped deposits of bright material can be seen in the images at L_s 20. The scene at L_s 57 appears to have been generally re-frosted, as older fans have disappeared and new ones emerged – Mars Express OMEGA data show that there is an optically thick layer of H_2O ice that gradually condenses on the CO_2 ice to the point that at L_s 50 the spectral signature of CO_2 is hidden (Appere et al., 2011). HiRISE cannot detect the difference between CO_2 and H_2O, but new H_2O frost deposition may explain the difference in appearance (older fans disappearing, new fans forming) between L_s = 37 and 57, in addition to the previously discussed possibilities. The crests of the dunes are largely defrosted by L_s 71.

2.2. Furrows as sources of fans

The activity that rings barchan dunes at the dune-substrate interface is a very typical seasonal phenomenon, illustrated in Fig. 9, first

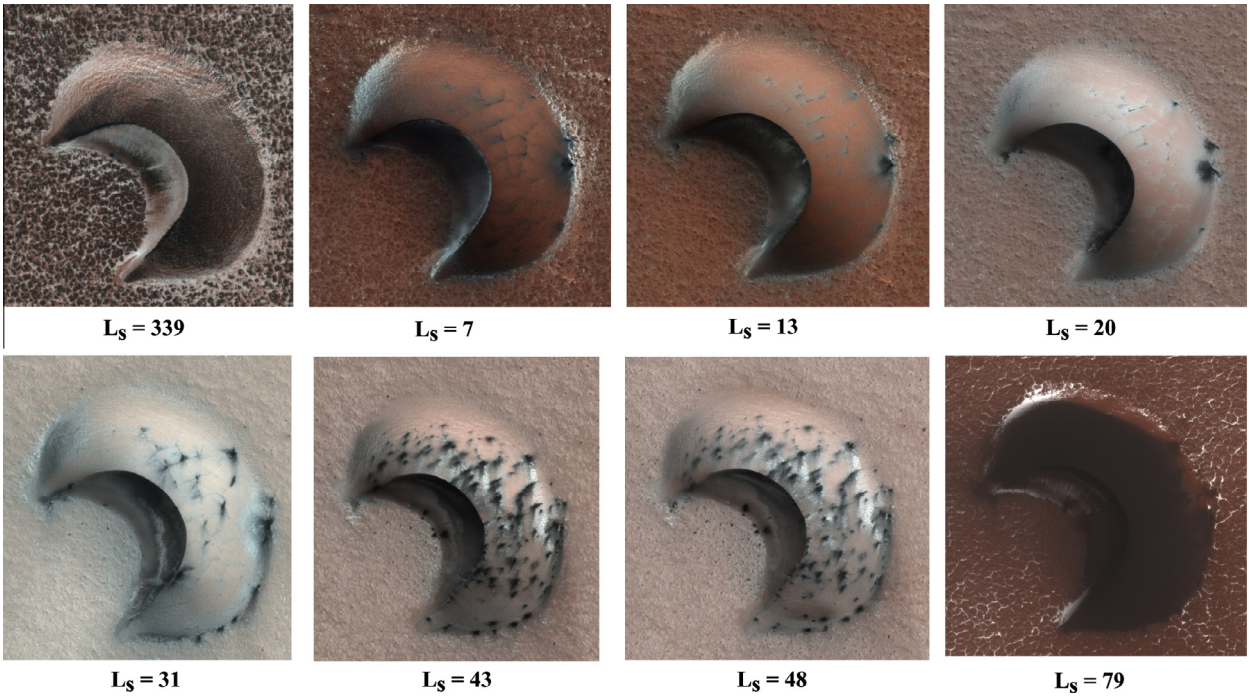

Fig. 6. This series of sub-images were acquired at 75.8N/94.055E. The sequence of seasonal activity illustrated is observed on numerous barchan dunes in the north polar erg. Images shown are (upper row, left to right) ESP_023536_2560, ESP_024235_2560, ESP_024380_2560, ESP_024591_2650, (lower row) ESP_024881_2650, ESP_025237_2650, ESP_025369_2650 and ESP_026292_2560 (which has been brightened relative to nominal RGB processing).

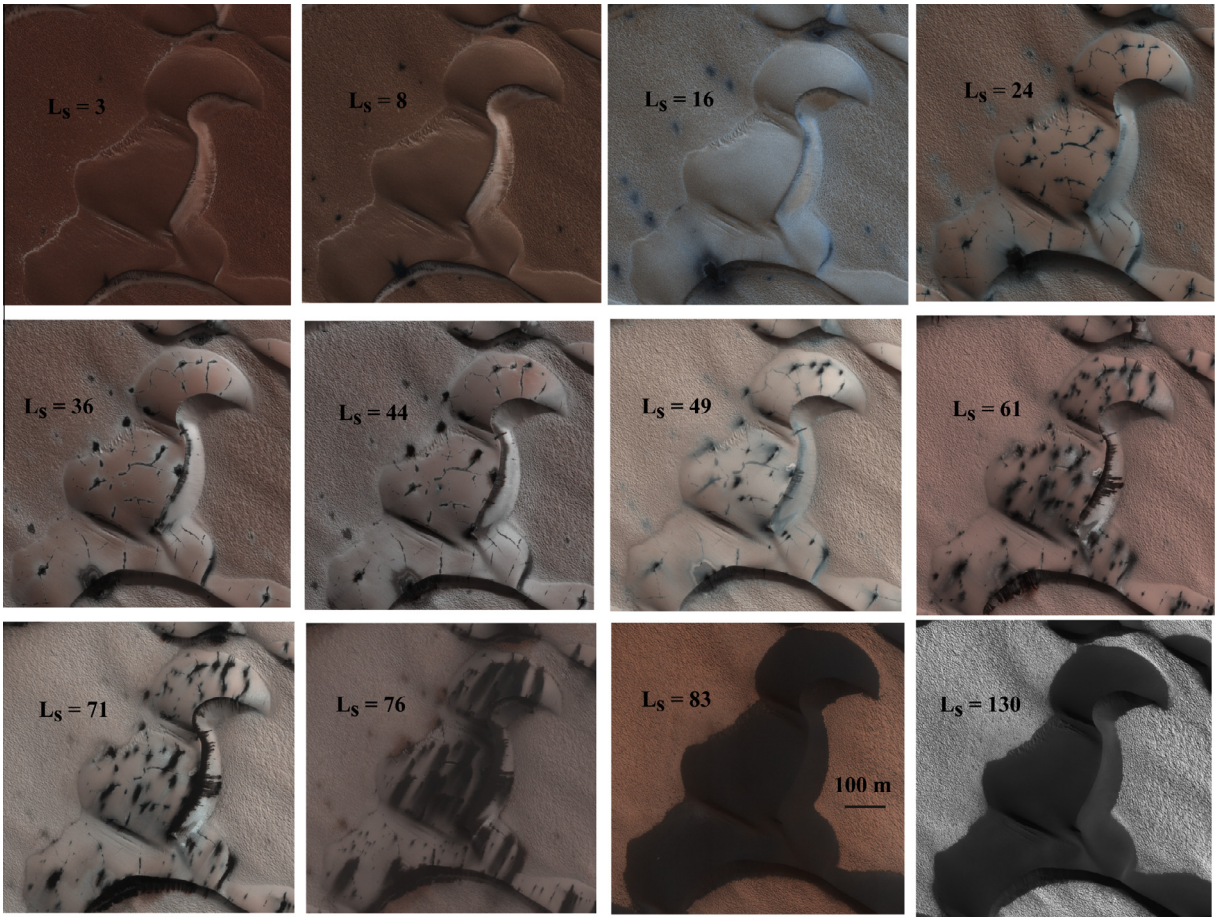

Fig. 7. Sub-images of the "Kolhar" dunes at 84.7N/0.7E are from (left to right): ESP_024119_2650, ESP_024264_2650, ESP_024475_2650, ESP_024699_2650, ESP_025042_2650, ESP_025253_2650, ESP_025398_2650, ESP_025754_2650, ESP_026031_2650, ESP_026176_2650, ESP_026387_2650, and ESP_027719_2650 (red filter only - not RGB). Defrosting of all slopes occurs rapidly between L_s 71 and 83.

noted in MOC images (Malin and Edgett, 2000). These outbreaks occur early in the spring. Fans continue to emerge throughout the spring. If the wind is not blowing they form somewhat circular features, but more typically fans extend outward from the interface, sometimes in multiple directions. Very long fans of dust may be deposited downwind. Note that spring winds are not always from the same direction that formed the dunes as indicated by the slipfaces – winter and spring winds have little effect on dune morphology because the dunes are protected by their layer of seasonal ice. Winds do have an effect on the ice on the dunes as described in the companion paper by Pommerol et al. (2013).

Furrows are shallow, branching and networked features on the surface of polar dunes (Bourke, submitted for publication). They are on average, 1.4 m wide and can extend the entire length of the windward slope (e.g. Fig. 2 in Hansen et al. (2011)). Mapping of furrow location between successive martian summers show that furrow placement on the dune changes each Mars year and is associated with the location of the polygonal crack pattern in the seasonal CO_2 ice (Bourke, submitted for publication). On at least some dunes we can see that outbreak locations in the seasonal ice are spatially correlated with furrow locations. Fig. 10 shows another example of furrows on one of the dunes in Arrakis. It is ringed with outbreaks in early spring. Time series of images show that material continues to emerge throughout the spring. The furrows are evidently acting as conduits for gas trapped below the seasonal ice to escape at the dune-substrate interface, entraining material from the dune.

2.3. Cracks as source of fans

2.3.1. Polygonal cracks

Polygonal cracks are observed in the ice on the dunes in almost every location we have imaged. Generally the cracks form on the relatively flat stoss side of the dunes, although polygonal cracks on the slipface of a dune in Arrakis have been observed. The timing at which they occur varies widely. Cracking of the seasonal ice layer is predicted by models of basal sublimation (Piqueux and Christensen, 2008; Portyankina et al., 2010, 2011), and lends more support to the hypothesis of gas trapped under partially translucent ice in the north as well as the south. Examples are shown in Fig. 11, in addition to Figs. 4, 6 and 7. A particularly nice example of polygonal cracking is shown in Fig. 12a. Fig. 12b shows that when the ice is gone the polygons are gone, confirming that the cracks are in the ice, not on the dunes.

2.3.2. Crestline cracks

Cracks also occur along the crest of the dune, providing dune sand an opening, as shown in Fig. 13, to move down the slipface in concentrated paths. Sand collects at the bottom of the slipface. As cracks elongate the slipface may appear sheathed in sand.

2.4. Sublimation-driven Mass wasting on dunes

In areas of the north polar erg with more abundant sand, barchanoid and transverse dunes are common. These dunes display

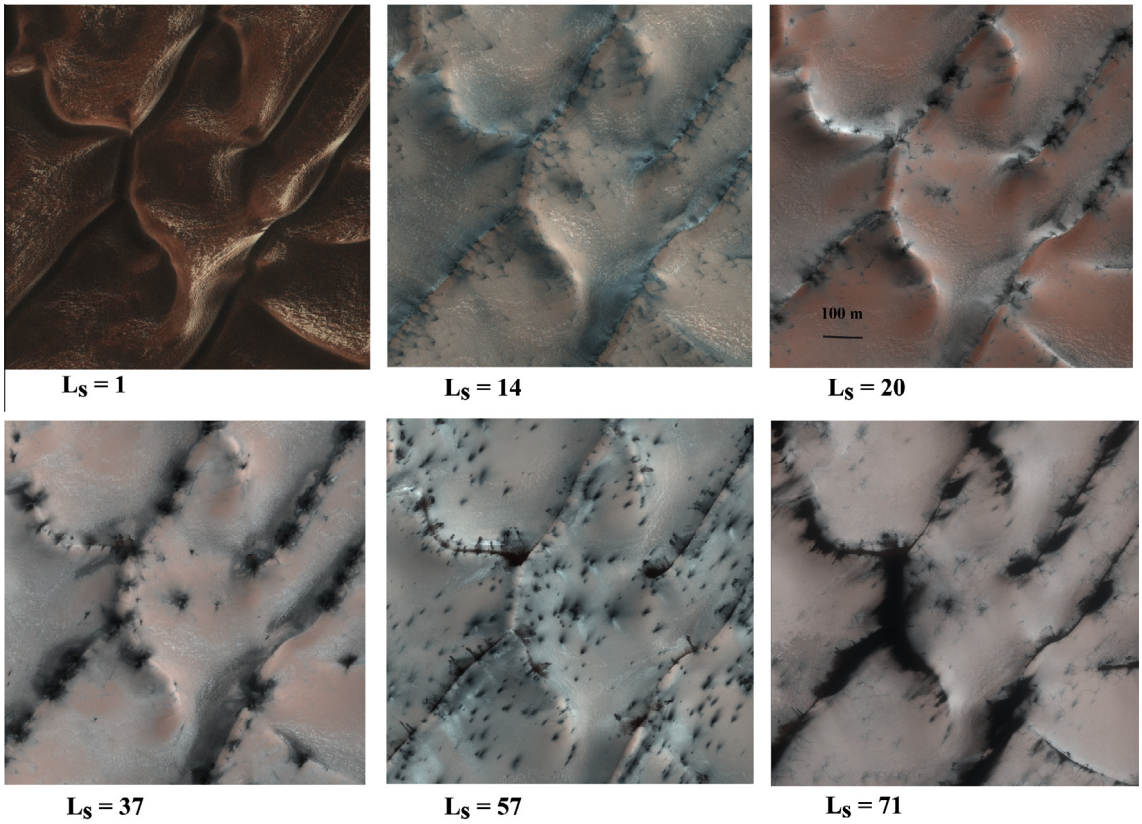

Fig. 8. This series of sub-images was acquired in study year 3 (MY31) at 80.22N/217.1E. The images shown (with incidence angles in parentheses) are, left to right, ESP_024072_2605 (80.4), ESP_024428_2605 (74.7), ESP_024573_2605 (72.5), ESP_025061_2605 (66.4), ESP_025628_2605 (60.6), and ESP_026050_2605 (58.0).

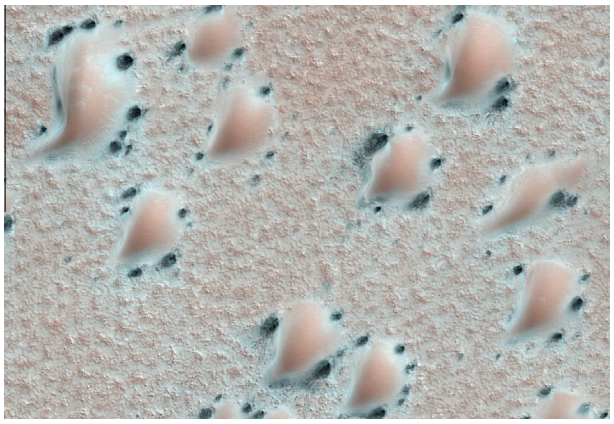

Fig. 9. "Outbreaks" of dune sand and dust ring these barchan dunes. This 1.3 km wide sub-image of ESP_024621_2535 at 73.35N/355.1E was acquired at L_s 21. Illumination is from the upper right as shown.

sand flows down slipfaces in the spring, mobilized by the destabilizing activity associated with the sublimation of CO_2. Fig. 14 shows numerous dark sand flows, including a dust cloud being raised by falling material (Hansen et al., 2011).

Sand flows are observed to appear and lengthen as the spring season progresses, guided by existing dune morphology. Möhlmann (2008) discuss the possibility that thin layers of interfacial water might be present in the dunes, reducing friction. Kereszturi et al. (2009) attribute the streaks to liquid brine flows, however liquid brine would be in direct association with CO_2 ice at ~145 K, and would have to stay liquid while flowing tens of meters. Our preferred explanation is gravity-driven mass wasting, initiated by CO_2 sublimation and gas flow. See Section 3 for further discussion.

2.5. Sand avalanches and dune erosion

Comparison of HiRISE images of ice-free dunes acquired in MY29 and MY30 showed sediment transport on the dunes. These images show substantial change in the form of new alcoves and debris aprons, association of changes with seasonal activity, and the reworking of the debris aprons by wind forming new ripples (Hansen et al., 2011), as shown in Fig. 15.

Some sand avalanches move hundreds of cubic meters of material (Hansen et al., 2011, SOM). New alcoves may be cut many meters into the existing dune brink. We hypothesize that gas flow from basal sublimation of the seasonal ice layer destabilizes the top of the dune. Fluidization of the eolian sediment by CO_2 sublimation has also been proposed (Hoffman, 2002; Cedillo-Flores et al., 2011). The Cedillo-Flores model requires mantling of the CO_2 frost by a layer of sand or dust. HiRISE images show that this is indeed possible (Fig. 14 for example) but more detailed analysis of where new alcoves are detected and whether they meet all the criteria for CO_2 fluidization is required.

In the third study year images show that alcoves are rapidly filled in, as illustrated in Fig. 16. A prominent alcove imaged in MY29 is entirely filled in by MY31. It is not clear at this time whether that is entirely due to sand transport by the wind, or whether the weight of the layer of seasonal ice is somehow helping to smooth out the sand on the slipface.

2.6. Bright–dark–bright banding

Another puzzling sublimation feature appears at the crests of dunes, along cracks on the stoss side of the dunes, and at the interfaces of the dune with the interdune substrate, illustrated in Fig. 17. Bright–dark–bright bands appear early in spring

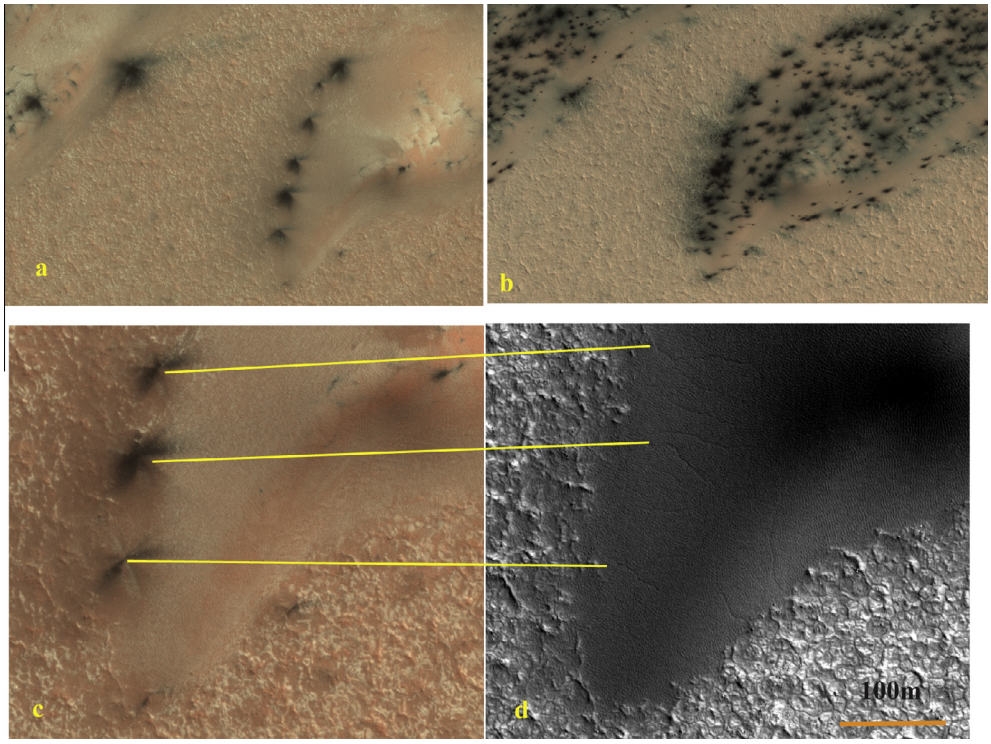

Fig. 10. (a) Outbreaks form early in the spring along the dune-substrate interface, as illustrated in ESP_016111_2600, taken at L_s 32.5. (b) More material has emerged, from more outbreaks, at L_s 54.5, ESP_016744_2600. (c and d) When all seasonal ice has sublimated small furrows in the dune are visible, shown in (d), ESP_018445_2600, taken at L_s 113.2. Comparison of the outbreaks in ESP_016111_2600 (c), to ESP_018445_2600 (d) shows the correlation of the outbreak sites to the furrows.

(L_s = 16–30) and fade slowly as the season progresses (also termed "rings," described in Kereszturi et al., 2010). These do not appear to be related to the morphology of the underlying surface. It may be that this is a particle-size effect, as discussed in the companion paper by Portyankina et al. (2013). It has been shown that different particle sizes will settle out at different distances from the source vent, and that the distribution depends on both slope and ambient wind (Fig. 16 in Thomas et al. (2011a)).

2.7. Non-dune terrain

In the north we have looked at regions suggested as likely sites of translucent ice (Piqueux and Christensen, 2008), to search for channels carved in the surface, similar to the araneiform terrain observed in the southern hemisphere (Piqueux et al., 2003; Hansen et al., 2010). We have not imaged (in the small sample of the surface imaged by HiRISE) any araneiform terrain.

In general, regions without dunes show very little sign of seasonal activity. Fig. 18 shows one exception, an example of a fan in the north in a region with no dunes. Fans in this region tend to be bright at blue wavelengths, indicative of frost condensing from gas rather than transport of fine dark surface material. It is likely that decompression and adiabatic cooling of pressurized gas being released from below the ice causes condensation of frost, which shows up as a fresh bright streak (Titus et al., 2007; Thomas et al., 2010). If basal sublimation is active then the nature of the surface apparently makes entrainment of surface material unlikely here.

3. Seasonal processes

3.1. Sublimation-driven mass wasting vs. salt brines

As the spring season progresses slope streaks/sand flows often lengthen. Fig. 19a–c show a temporal series of images of the same location. This may appear to lend credence to the Kereszturi hypothesis of salt brine liquid flow (Kereszturi et al., 2010) but there are a few inconsistencies that lead us to the conclusion this is dry mass wasting. The offset of one streak from the slipface downslope direction is consistent with wind carrying material; and the detached dark spots at the bottom show material that appears to have skipped across the surface.

Temperature, however, is the biggest issue for the salt brines model. This scene is covered with CO_2 ice at a temperature of ~145 K. The liquid will be in contact with the ice, if not at its source then all the way downslope to the bottom. It will also radiate to an atmosphere buffered to the CO_2 frost point of ~145 K. Although it is theoretically possible to achieve brine eutectic temperatures as low as 145 K for vanishingly small quantities of liquid (Chevrier and Altheide, 2008; Rivera-Valentin et al., 2012), the minimum confirmed (measured) temperatures are no lower than 200 K (Chevrier and Altheide, 2008; Möhlmann and Thomsen, 2011).

3.2. Application of the Kieffer model to the dunes of the north polar erg

Most seasonal activity imaged by HiRISE can be explained by the Kieffer model, which features basal sublimation of the seasonal ice layer. The key tenets of the Kieffer model are that ice is translucent and impermeable at times during the spring. Sunlight penetrating the ice warms the darker ground below, causing sublimation from the bottom of the ice layer (Kieffer et al., 2006; Kieffer, 2007; Pilorget et al., 2011). Models show that only 10% of incoming solar radiation is required to be absorbed in the surface to get basal sublimation started. The subsequent buildup of pressure of trapped gas will cause the ice to rupture at a weak spot or cause polygonal cracking (Piqueux and Christensen, 2008; Portyankina et al., 2011). It is clear from the overlying thickness of the seasonal ice layer (Table 2) that something is needed to propel dune material up and out on top of the seasonal ice layer. Analogous to the southern hemisphere, when a rupture occurs in

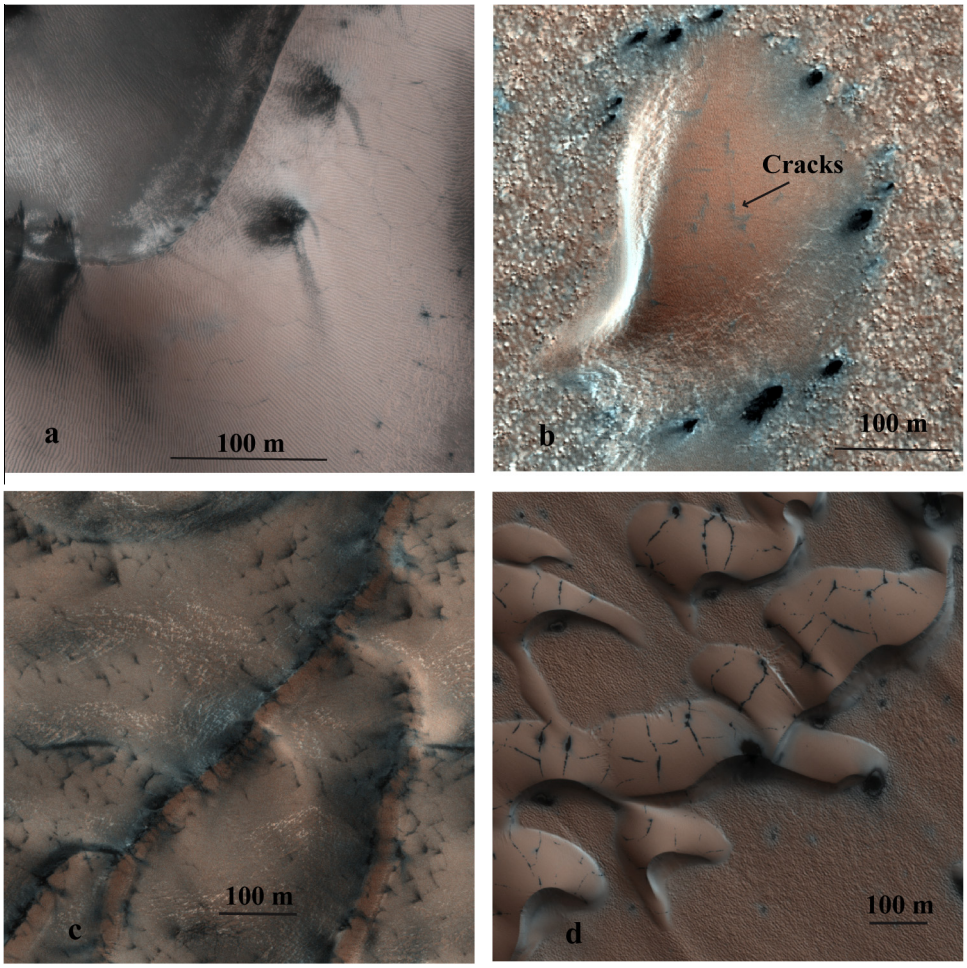

Fig. 11. Four different latitudes show cases of polygonal cracks forming in the overlying seasonal layer of ice: (a) ESP_024860_2525, acquired at 72.29N/311.75E, L_s 30; (b) ESP_024265_2535, acquired at 73.35N/355.1E, L_s 8; (c) ESP_024428_2605, acquired at 80.22N/217.1E, L_s 14; (d) ESP_024699_2650, acquired at 84.7N/0.7E, L_s 24. Cracks generally occur on the stoss side of the dune as shown for the barchan dunes on the right. They also occur in flatter regions of transverse dunes, shown on the left. Timing of their appearance varies widely. Sometimes (top right, arrow) just gas emerges from the crack, forming a bright line of re-condensed frost (contrast enhanced). More typically dust or sand from the dune is propelled out the crack to the top of the seasonal ice.

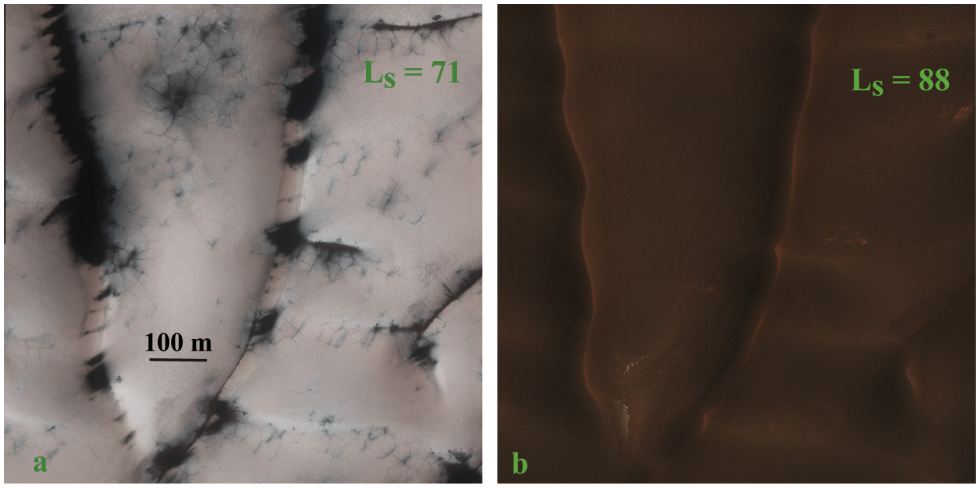

Fig. 12. (a) An example of polygonal cracks in the seasonal ice is shown from a sub-image of ESP_026050_2605, acquired at 80.22N/217E at L_s 71. (b) When the seasonal ice is gone polygonal cracks are no longer discernible, as shown in this sub-image of ESP_026551_2605, taken at L_s 88, confirming that the cracks are in the ice, not on the dunes.

the seasonal ice layer the pressurized gas will entrain surface material and carry it to the opening. After reaching the upper surface of the ice the material is carried away downwind and/or downslope.

Fig. 20 shows a cartoon of the model as envisioned for the dunes in the north. In HiRISE images we see three predominant weak spots: the crest, polygonal cracks on the stoss slope, and around the dune interface with the substrate.

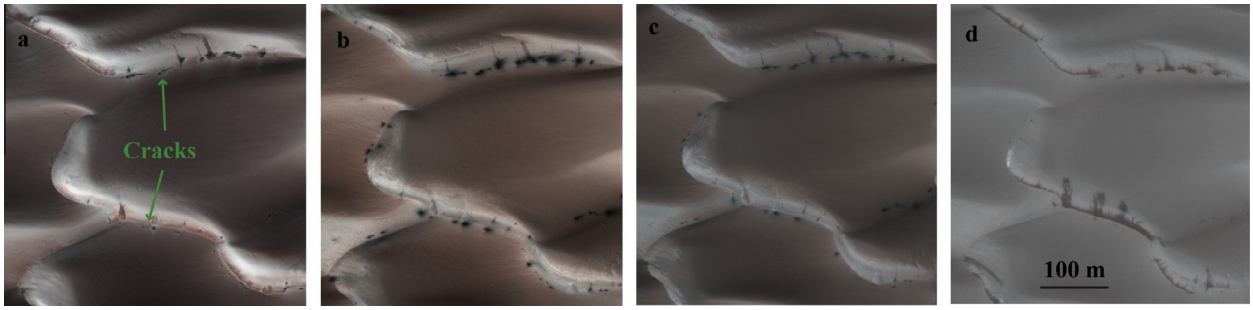

Fig. 13. This sequence acquired at 84N/233.2E ("Buzzel") shows the progression from the initial cracks along the crestline to sandfalls along the entire slipface. From left to right the images are ESP_025126_2640 at L_s 39.5, ESP_025416_2640 at L_s 49.6, ESP_025561_2640 at L_s 54.6, and ESP_025851_2640 at L_s 64.5. Sub-images a and d have been brightened relative to normal RGB processing.

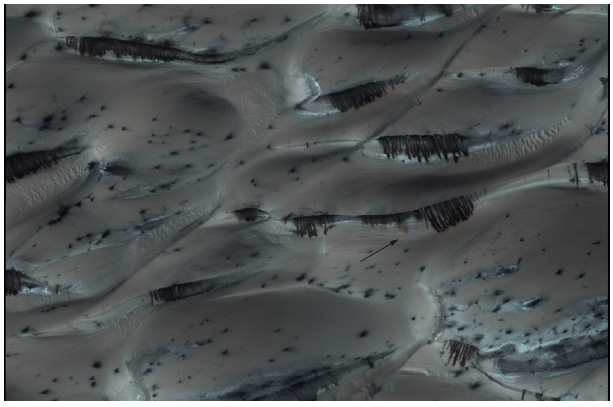

Fig. 14. Sand flows and a small cloud of dust (arrow) kicked up by falling material are captured in this sub-image of PSP_007962_2635, acquired at 83.5N/118.6E ("Tleilax"), at L_s 55.7. The dune with the dust cloud is ~40 m high, and the angle of the slipface is ~26°. North is up in this figure, illumination is from the lower left, and the entire image is ~1.3 km wide. The slipfaces are primarily oriented sunward.

3.2.1. Ice layer weak spots

The images show that the crest of the dunes is a weak spot – the ice there thins and cracks early in spring. In our hypothesized application of the Kieffer model to the northern dunes, seasonal frost sinters into competent ice sheets on the stoss and lee sides of the dune. A component of the weight of these sheets acts in the downhill direction (away from the crest and brink of the dune). Usually this downhill shear stress is balanced by friction with the underlying sand; however, if basal sublimation is occurring then the coefficient of friction may be reduced (or even eliminated) by pressure from the produced gas layer. At the top of the dune the weight of the ice acts downhill in diverging directions, which sets up tensional stresses in the ice at this location. These tensional stresses can widen and lengthen preexisting cracks creating a natural area for outgassing, which in turn mobilizes loose sand that gets ejected and deposited on top of the surrounding ice. Loose granular material on top of sublimating ice is rapidly fluidized (Cedillo-Flores et al., 2011) and flows easily down the slipface. Smaller particles are blown downwind from the opening at the crest.

More difficult to explain are the weak spots at the interface between the dune and the substrate. Perhaps differences in the material of the dune and the substrate lead to differential thermal expansion and contraction as the CO_2 is deposited, that disrupts the sintering process.

As discussed in Section 2.2 shallow furrows on barchan dunes lead to the dune-substrate interface (and occasionally to the crest) and can be correlated with locations of outbreaks of surface material. This may be the most analogous phenomenon in the north to the formation of the araneiform terrain in the south: gas funneled to a weak spot erodes and entrains surface material. Modeling indicates that sub-ice gas flow can reach 10 m/s, adequate to entrain 400 μm particles (Thomas et al., in preparation). The difference in the north is that the dune surface is only weakly consolidated and furrows may be erased by eolian sediment transport (Bourke, submitted for publication) rather than eroding more permanent channels.

3.2.2. Gas flow

Fig. 21 shows a typical example of fine material in fan-shaped deposits oriented in numerous directions. The similar directions of the numerous fans at different sources are consistent with the deposition direction of sand and dust being determined by winds that change direction over the duration of the gas release. This implies that (a) most of the vents open at the same time, and (b) they stay open or seal and re-open multiple times (Thomas et al., 2010). Fluid dynamics models show that it is possible to maintain gas flow after the vent has opened with adequate pressure to entrain surface material, leading to new fans pointed in different orientations as the wind direction varies (Thomas et al., 2011a). Steady state flow can produce fans that are 5–25 m in length (Thomas et al., 2011b).

3.3. Frost budgets and timing of activity

It seems clear that much of the activity described is being driven by CO_2 frost and its removal. We would therefore like to understand better when seasonal frost exists on dune slopes (both stoss and lee). Insolation, and by extension seasonal frost budgets, depends on terrain slope and aspect (defined to increase to the east with north as zero). This dependence becomes more sensitive as one approaches the pole. Fig. 22 illustrates the variability in total annual insolation incident on surfaces of a given slope and aspect. In the mid-latitudes, pole- and equator-facing slopes generally receive less or more insolation than adjacent flat terrain respectively, whereas at the pole itself any sloping surface receives more insolation than flat terrain. In regions close to the pole, this behavior becomes more complex. In the latitude range of interest (80–85°N), most slopes receive more insolation than flat terrain. However, some counter-intuitive peculiarities exist, for example a north-facing lee slope of a dune (34°) at 85°N receives approximately the same amount of sunlight as adjacent flat terrain when totaled over the whole year (Fig. 22). The seasonal distribution of when this energy arrives though is quite different. Fig. 23 breaks out some parts of the year within the defrosting season for closer inspection. Although terrain aspect matters little after L_s 20, it has a dominant effect within the crucial defrosting season from L_s 350–20.

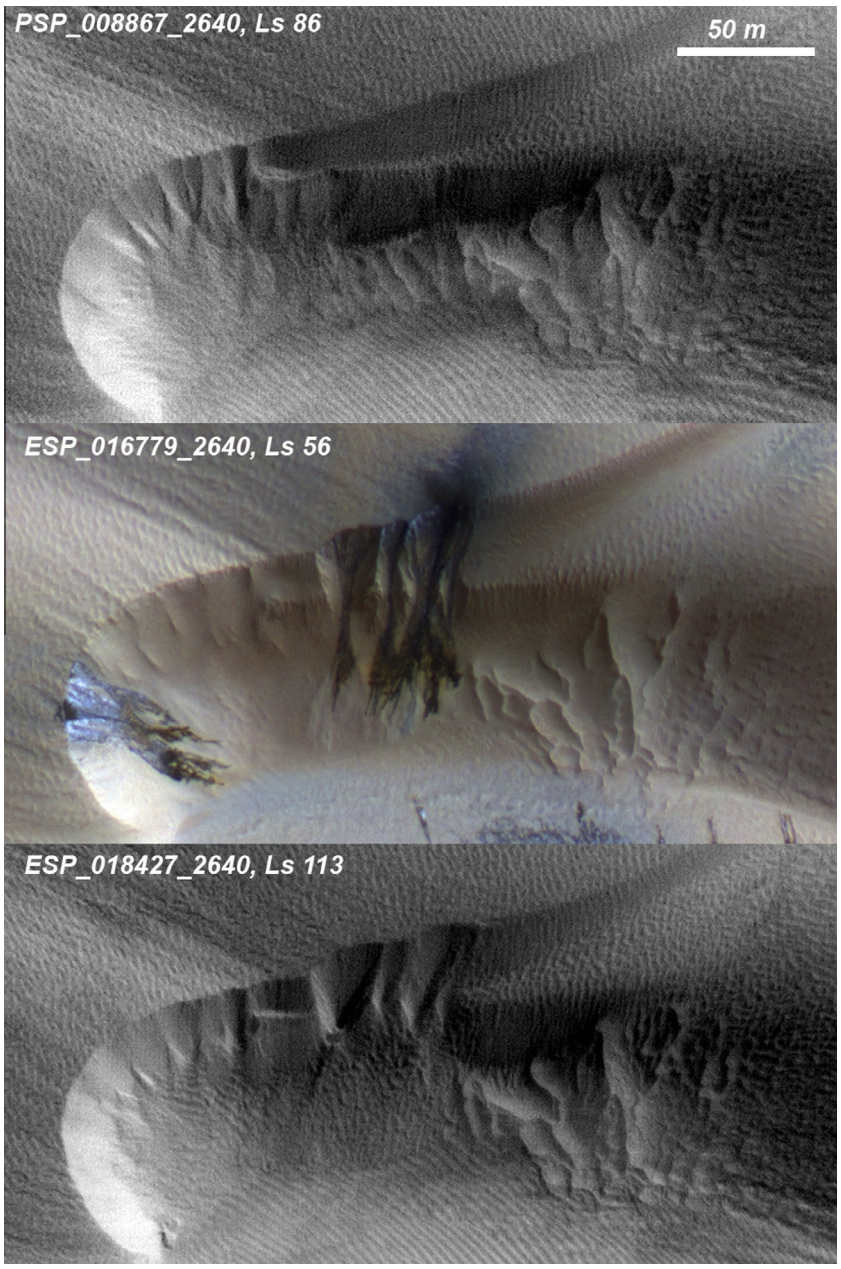

Fig. 15. These three images taken at 84N/233.2E ("Buzzel") depict the before and after morphology of a dune in one Mars year, and show association of seasonal activity with the new alcoves. The top image was taken first, in the martian summer when the dunes were free of seasonal ice. The middle image was acquired in the spring and shows typical seasonal activity at the location of the new alcoves. The bottom image shows the new alcoves and their debris aprons. New ripples have already started to form on the new debris aprons. This particular image set does not show when in the intervening year the gullies formed.

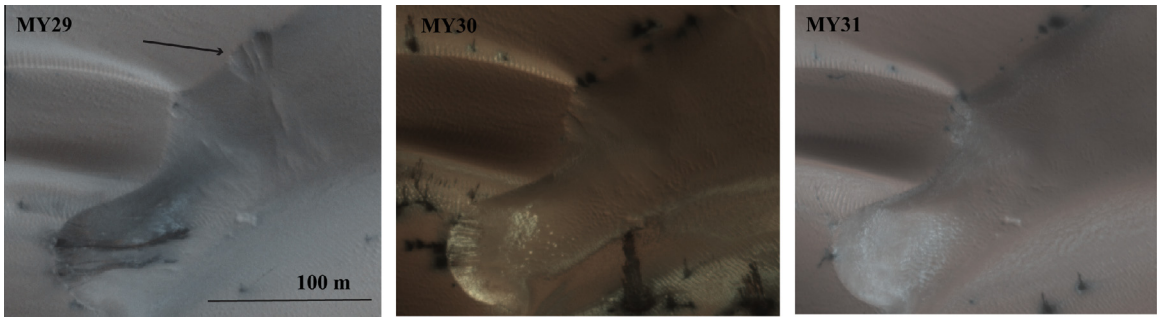

Fig. 16. An alcove several meters deep, indicated by the arrow, at 84N/233.2E ("Buzzel") has been erased in less than 2 Mars years. The MY29 sub-image is from PSP_007905_2640, taken at L_s 54. The alcove is barely discernible in the MY30 sub-image of ESP_016779_2640, taken at L_s 56. The alcove is gone in the MY31 sub-image of ESP_025561_2640, taken at L_s 55.

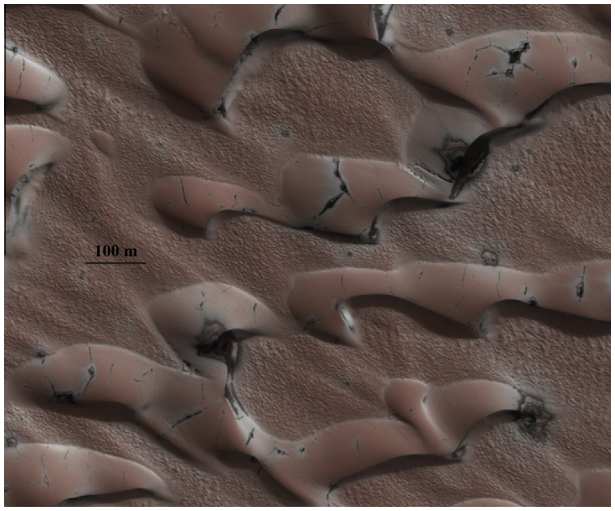

Fig. 17. Bright–dark–bright sublimation patterns are illustrated in this sub-image of ESP_025042_2650, acquired at 84.7N/0.7E ("Kolhar"), L_s 36.6. Bright–dark–bright banding in this location can be seen on the crest of the dune, at the dune-substrate interface, and even surrounding the cracks on the stoss side of the dunes.

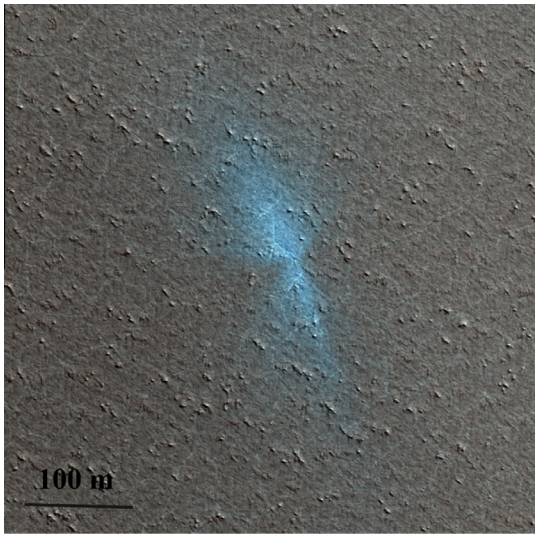

Fig. 18. This sub-image of PSP_007181_2655, acquired at 85.4N/180.5E, L_s 28.4 shows a bright fan.

We examine the seasonal behavior of the frost in these high latitude locations by simulating the surface temperature with a standard thermal diffusion model similar to that employed by Dundas and Byrne (2010) and based on a long line of such models (e.g. Kieffer et al., 1977). We balance incoming shortwave radiation, longwave atmospheric emission (assumed to be 4% of the noontime shortwave flux (Aharonson and Schorghofer, 2006; Haberle and Jakosky, 1991); but reduced by $\cos^2$(slope/2) for sloping surfaces, which see less sky), conductive exchange with subsurface layers and outgoing emitted longwave radiation. Incoming shortwave radiation is calculated for each slope and aspect of interest. Self-shadowing of the terrain may occur, but the model is only one-dimensional and shadows cast from nearby topography are neglected. We run the model first to simulate the temperature, albedo and emissivity (all of which change as frost comes and goes) of flat terrain with constraints described below. We use this flat terrain history to calculate scattered shortwave radiation and emitted longwave radiation incident on the sloping surfaces from surrounding terrain. To do this we assume that these slopes are surrounded by an infinite flat plane that behaves like our simulated flat terrain and scatters like a Lambert surface, i.e. the slopes receive a flux of $\pi \sin^2$(slope/2) times the radiance leaving each square meter of flat terrain.

If surface temperature falls below the frost point at that season (determined from a scaled version of the Viking lander pressure curve) then we hold the surface temperature constant at that value and allow CO_2 ice to accumulate or ablate in response to energy balance at the surface and conducted heat from below. We utilize thermophysical parameters common to porous basaltic sandy surfaces on Mars i.e. albedo 0.15, emissivity 0.95, thermal inertia 220 J m^{-2} K^{-1} S$^{-0.5}$, density 1650 kg m^{-3} and heat capacity of 837 J kg^{-1} and keep these parameters constant with depth. Variation of these parameters within reasonable bounds does not affect the results on peak frost depth and timing in a significant way. Previous suggestions of anomalously low thermal inertias in the Olympia Undae (Paige et al., 1994) appear explainable by the presence of buried ice (Putzig et al., 2010). The depth of this ice depends on the slope and aspect of the terrain (Schorghofer and Aharonson, 2005; Aharonson and Schorghofer, 2006) and atmospheric water vapor content, so inclusion of its effects in a self-consistent way requires a broader modeling effort than undertaken here. We do not include any buried ice in the following simulations, which would make our frost budgets erroneously large. In the following paragraph we explain how we compensate for this. Finally, layer thickness, maximum depth, and timestep in the mod-

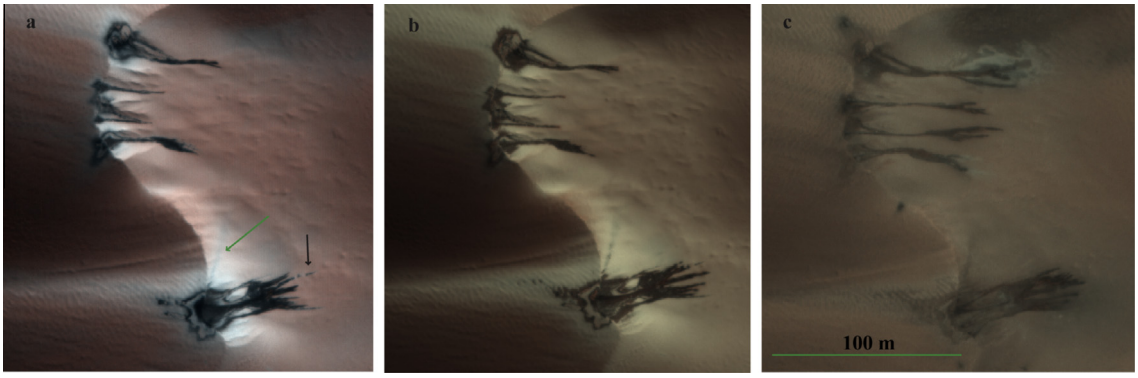

Fig. 19. (a) Evidence that slope streaks are caused by mass-wasting. In general the fines flow downhill guided by the dune morphology, but one streak jutting out to the side was apparently directed by the wind (green arrow). Detached dark spots at the bottom of the slope streaks show that material appears to have skipped across the surface (black arrow). This is a sub-image of PSP_007193_2640, taken at 84.0N/233.2E, L_s 28.8. The bright–dark–bright banding is common, as discussed in Section 2.6. (b) PSP_007404_2640, acquired at L_s 36, shows lengthening streaks. (c) PSP_007905_2640, acquired at L_s 53.8. Contrast between the frost-covered surface and the slope streak material from the sand dune is beginning to fade. Some new bright frost appears to have condensed around the distal end of the uppermost streak, which has lengthened and branched. (For interpretation of the references to color in this figure legend, the reader is referred to the web version of this article.)

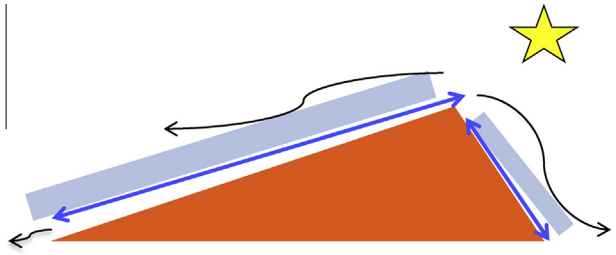

Fig. 20. Ice (gray bars) thins and cracks at the crest of the dune, exposing sand and dust, which is mobilized by the gas flow (blue arrows) from under the ice layer. Material cascades down the slip face and/or is blown out over the stoss side of the dune (black arrows). Large flat expanses of sand (such as the stoss) covered by ice are susceptible to polygonal cracking as the pressure of the gas from basal sublimation builds. (For interpretation of the references to color in this figure legend, the reader is referred to the web version of this article.)

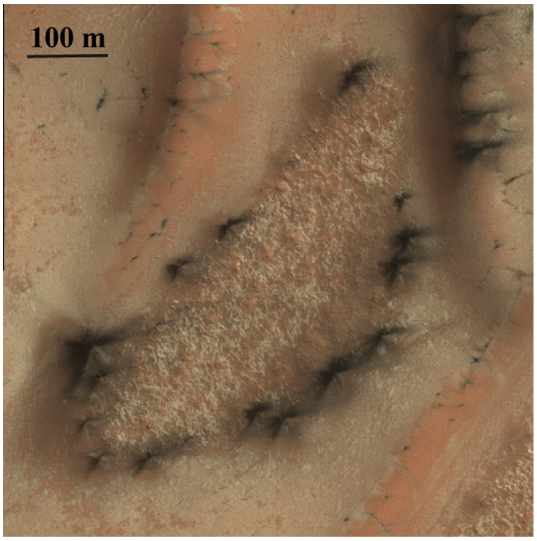

Fig. 21. This sub-image of ESP_016032_2600, acquired in Arrakis (Fig. 2b) at 80N/122.5E, L_s 29.7, shows multiple streaks from individual sources with similar directional patterns, and with the same relative sizes.

el were chosen to fully resolve the diurnal and annual thermal wave and maintain numerical stability through a Courant criterion.

The peak frost mass and timing is most sensitive to the combined effects of frost albedo and emissivity. We take observations of peak frost mass from the GRS results reported by Kelly et al. (2006) and adjust frost emissivity to 0.65 to reproduce this for flat terrain within our model. This emissivity is anomalously low; the actual physical reason for the low frost budgets is the buried ground ice that we neglected. Thus, we use frost emissivity to approximate the effects of buried ground ice (as GCM models did before ground ice was included in their calculations (Haberle et al., 2008)). We then varied frost albedo until our modeled flat terrain at 80°N defrosted at the correct season. Arrakis (80°N/122.5°E) still has visible frost at L_s 82, while another observation at that latitude (but at 217°E) shows bare ground at L_s 88. We pick the mid-point (L_s 85) to be the defrosting season at that latitude. The frost albedo, which yields this defrosting date is found to 0.72 and we employ this value in all the following runs. In reality, frost albedo and emissivity are not constant with season or location (Byrne et al., 2008; Titus et al., 2001). For the purposes of comparing differently sloped surfaces to each other we have neglected this variation. We examine time-variable frost albedo in a companion paper (Portyankina et al., 2013).

We defer to future work a full treatment of additional effects such as buried ground ice and time-variable frost albedo. The results reported here are intended to facilitate comparison between differently sloped terrains rather than be the most accurate possible representation of Mars itself.

Fig. 24 illustrates the seasonal frost expected to accumulate on the lee (at the angle of repose, 34°) and stoss (slopes of 5–10°) sides of a dune at 80°N as a function of aspect. As expected from the preceding discussion, aspect plays a crucial role in determining frost behavior. In a scene with dunes of many orientations we should expect a great variety of frost-driven activity. We find that flat terrain here has a peak frost mass of 708 kg m^{-2} at L_s 10 (tuned via frost emissivity to approximately match the GRS results of Kelly et al. (2006)). The sloping dune faces accumulate more and defrost later when north-facing and vice versa when south-facing. A 10° stoss slope may accumulate anywhere between 598 and 810 kg m^{-2} depending on its aspect and have its peak frost load anytime between L_s 357 and 17. This behavior becomes even more extreme for the steeper lee slopes (34°). Steep south-facing lee faces accumulate only 491 kg m^{-2} and start losing frost as early as L_s 339 (such is the quantity of the heat they absorbed during the previous summer), whereas steep north-facing lee faces accumulate 773 kg m^{-2} and do not start to lose frost until L_s 18.

The season in which final defrosting is expected follows similar trends to peak frost timing (Fig. 25). All modeled slopes defrosted by L_s 91. Lee slopes are expected to lose their frost covering between L_s 43 and 86 while frost on 10° stoss slopes disappears

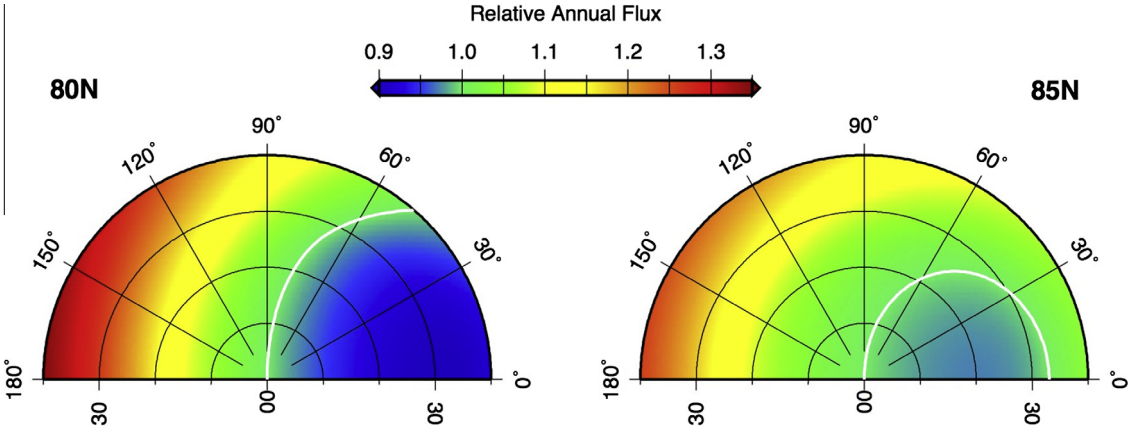

Fig. 22. Total annual insolation for a sloping surface at 80°N (left) and 85°N (right). Insolation has been normalized to the total incident at flat terrain at these latitudes. The white contour has a value of 1.0 i.e. equivalent to the flat terrain insolation. Slope is the radial coordinate and aspect the azimuthal.

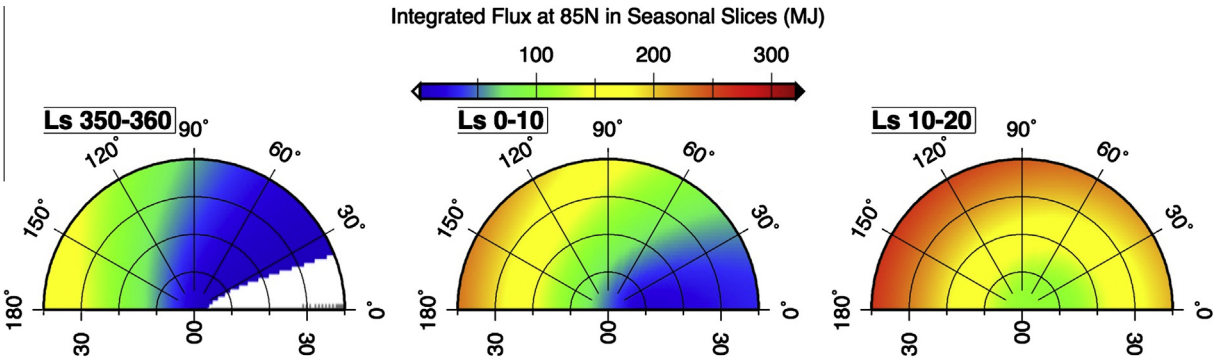

Fig. 23. Integrated insolation as a function of slope and aspect (formatted as in Fig. 22) in three seasonal slices (left to right, L_s 350–360, 0–10, 10–20) with common color scale.

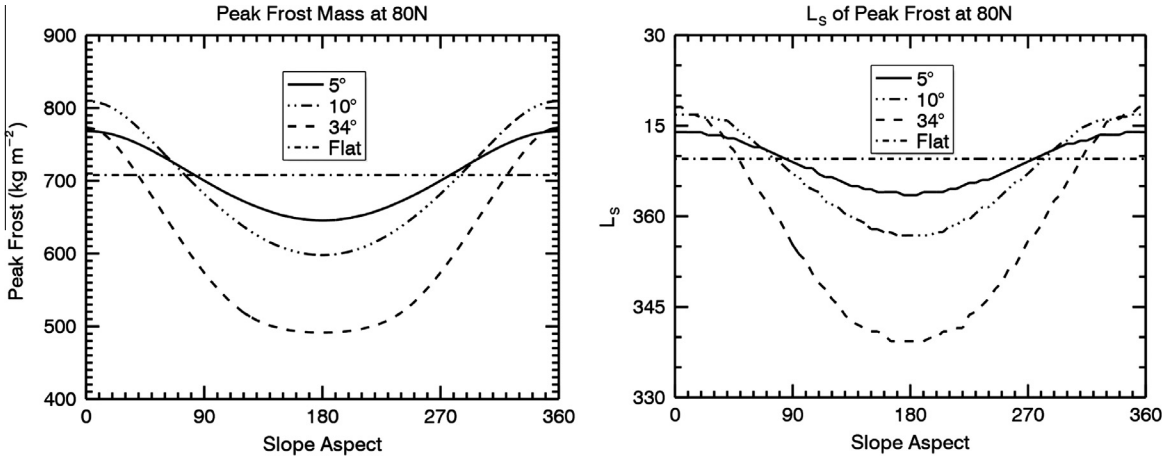

Fig. 24. Peak frost mass (left) and timing (right) as a function of slope aspect. Stoss sides have slopes 5–10° and lee sides ~34°. Flat terrain behavior shown for comparison.

between L_s 76 and 91. In contrast, flat terrain defrosts at L_s 85 (as we forced it to in order to agree with observations). Fig. 25 shows that defrosting dates vary most between slopes when they are south-facing; in contrast, north-facing slopes all defrost in a narrow seasonal range. It is interesting to note though that pole-facing stoss slopes collect more frost than pole-facing lee slopes (Fig. 24) even though they defrost at approximately the same time.

3.4. Examples of spring defrosting

Inspection of Fig. 25 shows several trends that should be apparent in the images. Consider a dune that has a south-facing slipface (slope aspect of 180 for a 34° slope). The slipfaces oriented to the south will lose their cover of seasonal ice much earlier (as early as L_s 50) than the north-facing gradually-sloping stoss side of the same dunes. In contrast, a dune with a north-facing slipface will lose the seasonal ice cover across the entire dunefield at closer to the same time: L_s 80 for the south-facing stoss side, L_s 90 for the slipface.

Fig. 26 illustrates the spring defrosting sequence of a dune field at 81N/156E. At L_s 0.4 the entire dune field is covered with its layer of seasonal CO_2. As spring progresses cracks and fans appear. The more southward-facing gradually-sloping stoss side of the dunes has begun to defrost around L_s 70. At L_s 85 only the steep northward-facing slopes retain their frost cover.

Consistent with predictions, Fig. 8 shows for south-facing slipfaces, that the upper part of the slipface is ice-free at L_s = 57 while shallower slopes are defrosting at L_s = 71. Flatter ground is still

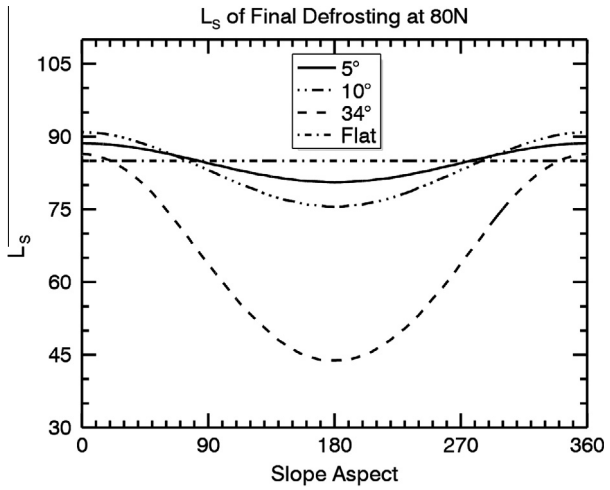

Fig. 25. Final defrosting season as a function of slope aspect, formatted as in Fig. 24.

frosted, as expected. By L_s = 88 (Fig. 11b) the entire dunefield is ice-free.

4. Summary and comparison to southern seasonal phenomena

In the north, as in the south, spring sublimation of the seasonal CO_2 polar cap is a dynamic process. In the north activity is

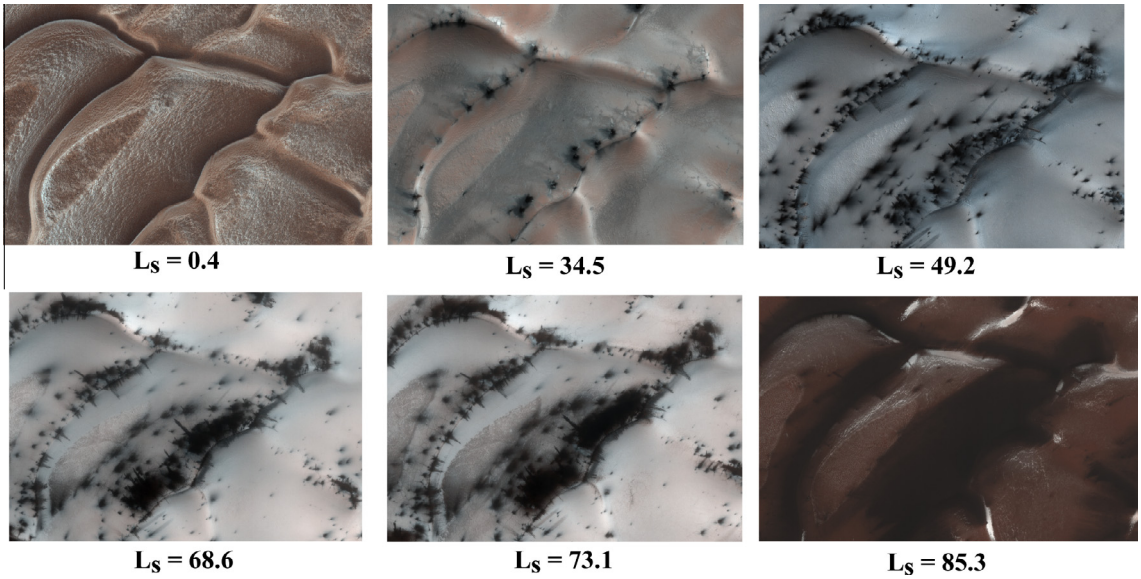

Fig. 26. The sub-images shown here are 1.3 km across, from the dune field known informally as "Zanovar," at 81.0N/156.0E. They are, from left to right, upper row, ESP_024061_2610, ESP_024984_2610, ESP_025406_2610, lower row, ESP_025973_2610, ESP_026105_2610, and ESP_026461_2610.

concentrated on the dunes. Dune stoss and lee slopes play a major role in the way that spring activity progresses.

We find that the Kieffer basal sublimation model, well-developed to explain southern sublimation processes, is consistent with and provides a good explanation for the activity imaged in the north. Fans of dark surface material (dune sand in the north) propelled to the top of the ice layer by escaping gas are deposited in directions determined by the prevailing wind and/or slope. Bright fans form in the north also, and like in the south form only in limited time intervals, apparently when conditions are just right.

Three main weak spots are identified for gas escape on the dunes: the crest, the dune-ground interface, and polygonal cracks on the stoss. Polygonal cracking is also seen in the southern hemisphere. The physics at the crest of the dune are likely the same as at the channel edges in southern araneiform terrain: an inherent weakness due to underlying topography and the early exposure to sunlight. There are no southern counterparts to the outbreaks we see at the dune-substrate interface, or the bright–dark banding.

Furrows on dunes in the north are probably the counterpart to the araneiform channels in the south, moving trapped gas to the nearest opening; however, unlike in the south they are not permanently carved into the surface.

Sand flows from the dune crests are attributed to the release of gas from basal sublimation through cracks in the ice along the dune crest. This cover of sand may provide the mantle required for CO_2 fluidization after burial, which might in turn be the cause of the large new alcoves. More work remains to validate that the conditions for CO_2 fluidization can be met. Large (meters deep) alcoves can be erased in <3 Mars years.

All the different dune slopes add a complexity that can be modeled, for insolation distribution on a variety of aspect angles. These predictions can be used to predict peak frost and L_s of final sublimation of the frost. The more complex model we have envisioned for the future will in turn be compared to observations to derive frost properties such as albedo and emissivity, and distribution of ground ice.

Landscape evolution is occurring on Mars today, in the current climate, driven by sublimation of the seasonal CO_2 polar cap.

Acknowledgments

We were fortunate to have Hugh Kieffer (originator of the "Kieffer Model" described herein, and a mentor to several of us) as one of our reviewers. We are very appreciative of his time, and especially his effort to replicate our results, which led to substantial improvements to this paper. We also thank an anonymous reviewer for their positive comments. This work was supported by the Mars Reconnaissance Orbiter mission at the Jet Propulsion Laboratory, California Institute of Technology, under contracts with the National Aeronautics and Space Administration.

References

Aharonson, O., Schorghofer, N., 2006. Subsurface ice on Mars with rough topography. J. Geophys. Res. 111, 11007. http://dx.doi.org/10.1029/2005JE002636.

Aharonson, O., Zuber, M.T., Smith, D.E., Neumann, G.A., Feldman, W.C., Prettyman, T.H., 2004. Depth, distribution and density of CO_2 deposition on Mars. J. Geophys. Res. 109, E05004. http://dx.doi.org/10.1029/2003JE002223.

Appere, T. et al., 2011. Winter and spring evolution of the northern seasonal deposits on Mars from OMEGA on Mars Express. J. Geophys. Res. 116, E05001. http://dx.doi.org/10.1029/2010JE003762.

Bourke, M.C., submitted for publication. Seasonal formation of furrows on martian polar dunes.

Bourke, M.C., Balme, M., Beyer, R.A., Williams, K.K., Zimbelman, J., 2006. A comparison of methods used to estimate the height of sand dunes on Mars. Geomorphology 81, 440–452.

Boynton, W.V. et al., 2003. Constraints on the distribution of hydrogen in the polar regions of Mars and implications for ice formation processes. AGU. Abstract P32-B05.

Byrne, S., Murray, B.C., 2002. North polar stratigraphy and the paleo-erg of Mars. J. Geophys. Res. 107. http://dx.doi.org/10.1029/2001JE001615, 11-1.

Byrne, S., Zuber, M.T., Neumann, G.A., 2008. Interannual and seasonal behavior of martian residual ice-cap albedo. Planet. Space Sci. 56, 194–211.

Cedillo-Flores, Y., Treiman, A.H., Lasue, J., Clifford, S.M., 2011. CO_2 gas fluidization in the initiation and formation of martian polar gullies. Geophys. Res. Lett. 38, L21202. http://dx.doi.org/10.1029/2011GL049403.

Chevrier, V.F., Altheide, T.S., 2008. Low temperature aqueous ferric sulfate on the surface of Mars. Geophys. Res. Lett. 35, L22101. http://dx.doi.org/10.1029/2008GL035489.

Clancy, R.T. et al., 2000. An intercomparison of ground-based millimeter, MGS, TES, and Viking atmospheric temperature measurements: Seasonal and interannual variability of temperatures and dust loading in the global Mars atmosphere. J. Geophys. Res. 105, 9553–9571.

Coleman, S.J., Hayward, R.K., 2011. A higher resolution update to Viking-based martian north polar dune slipface analyses. Lunar Planet. Sci. 42. Abstract #1436.

Cutts, J.A., Blasius, K.R., Briggs, G.A., Carr, M.H., Masursky, H., Greeley, R., 1976. North polar region of Mars – Imaging results from Viking 2. Science 194, 1329–1337.

Delamere, W.A. et al., 2010. Color imaging of Mars by the High Resolution Imaging Science Experiment (HiRISE). Icarus, 205, 38–52.

Diniega, S., Byrne, S., Bridges, N.T., Dundas, C.M., McEwen, A.S., 2010. Seasonality of present-day martian dune gully activity. Geology 38, 1047–1050.

Dundas, C., Byrne, S., 2010. Modeling sublimation of ice exposed by new impacts in the martian mid-latitudes. Icarus 206, 716–728.
Farmer, C.B., Doms, P.E., 1979. Global and seasonal variation of water vapor on Mars and the implications for permafrost. J. Geophys. Res. 84, 2881–2888.
Garvin, J.B., Frawley, J.J., Sakimoto, S.E.H., 1999. North polar dunes on Mars: MOLA measurements and implications for sediment volumes. Lunar Planet. Sci. 30. Abstract #1721.
Haberle, R.M., Jakosky, B.M., 1991. Atmospheric effects on the remote determination of thermal inertia on Mars. Icarus 90, 187–204.
Haberle, R.M. et al., 2008. The effect of ground ice on the martian seasonal CO_2 cycle. Planet. Space Sci. 56, 251–255.
Hansen, C.J., Thomas, N., Portyankina, G., McEwen, A.S., Becker, T., Byrne, S., Herkenhoff, K., Kieffer, H., Mellon, M., 2010. HiRISE observations of gas sublimation-driven activity in Mars' southern polar regions: I. Erosion of the surface. Icarus 205, 283–295.
Hansen, C.J. et al., 2011. Seasonal erosion and restoration of Mars' northern polar dunes. Science 331, 575–578.
Hayward, R.K. et al., 2008. Mars global digital dune database: Distribution in north polar region and comparison to equatorial region. Lunar Planet. Sci. 39. Abstract #1208.
Hayward, R.K., Fenton, L.K., Tanaka, K.L., Titus, T.N., Colaprete, A., Christensen, P.R., 2010. Mars Global Digital Dune Database; MC1: U.S. Geological Survey Open-File Report 2010-1170. <http://pubs.usgs.gov/of/2010/1170/>.
Hoffman, N., 2002. Active polar gullies on Mars and the role of carbon dioxide. Astrobiology 2, 313–323. http://dx.doi.org/10.1089/153110702762027899.
Horgan, B.H.N., Bell, J.F., 2012. Seasonally active slipface avalanches in the north polar sand sea of Mars: Evidence for a wind-related origin. Geophys. Res. Lett. 39, L09201.
Kelly, N.J. et al., 2006. Seasonal polar carbon dioxide frost on Mars: CO_2 mass and columnar thickness distribution. J. Geophys. Res. 111, E03S07. http://dx.doi.org/10.1029/2006JE002678.
Kereszturi, A. et al., 2009. Recent rheologic processes on dark polar dunes of Mars: Driven by interfacial water? Icarus 201, 492–503.
Kereszturi, A., Möhlmann, D., Berczi, Sz., Ganti, T., Horvath, A., Kuti, A., Sik, A., Szathmary, E., 2010. Indications of brine related local seepage phenomena on the northern hemisphere of Mars. Icarus 207, 149–164.
Kieffer, H.H., 2000. Annual punctuated CO_2 slab-ice and jets on Mars. LPI Contribution #1057.
Kieffer, H., 2007. Cold jets in the martian polar caps. J. Geophys. Res. 112, E08005.
Kieffer, H.H., Titus, T.N., 2001. TES mapping of Mars' north seasonal cap. Icarus 154, 162–180.
Kieffer, H.H., Martin, T.Z., Peterfreund, A.R., Jakosky, B.M., Miner, E.D., Palluconi, F.D., 1977. Thermal and albedo mapping of Mars during the Viking primary mission. J. Geophys. Res. 82, 4249–4291.
Kieffer, H.H., Christensen, P.R., Titus, T.N., 2006. CO_2 jets formed by sublimation beneath translucent slab ice in Mars' seasonal south polar ice cap. Nature 442, 793–796.
Lancaster, N., Greeley, R., 1990. Sediment volume in the north polar sand seas of Mars. J. Geophys. Res. 95, 10921–10927.
Langevin, Y. et al., 2007. Evolution of the seasonal caps of Mars observed by OMEGA on Mars Express. In: *Seventh International Conference on Mars*, LPI 1353. p. 3246.
Leighton, R.B., Murray, B.C., 1966. Behavior of carbon dioxide and other volatiles on Mars. Science 153, 136–144.
Litvak, M.L. et al., 2007. Long-term observations of southern winters on Mars: Estimations of column thickness, mass, and volume density of the seasonal CO_2 deposit from HEND/Odyssey data. J. Geophys. Res. 112, E03S13.
Malin, M.C., Edgett, K.S., 2000. Frosting and defrosting of martian polar dunes. Lunar Planet. Sci. XXXI. Abstract #1056.
Malin, M.C., Edgett, K.S., 2001. Mars Global Surveyor Mars orbiter camera: Interplanetary cruise through primary mission. J. Geophys. Res. 106, 23429–23570.
Malin, M.C. et al., 1998. Early views of the martian surface from the Mars Orbiter Camera of Mars Global Surveyor. Science 279, 1681–1685.
Massé, M., Bourgeois, O., Le Mouelic, S., Verpoorter, C., Le Deit, L., Bibring, J.-P., 2010. Martian polar and circum-polar sulfate-bearing deposits: Sublimation tills derived from the North Polar Cap. Icarus 209, 434–451.
Massé, M., Bourgeois, O., Le Mouelic, S., Verpoorter, C., Spiga, A., Le Deit, L., 2012. Wide distribution and glacial origin of polar gypsum on Mars. Earth Planet. Sci. Lett. 317–318, 44–55.
Matsuo, K., Heki, K., 2009. Seasonal and interannual changes of volume density of martian CO_2 snow from time-variable elevation and gravity. Icarus 202, 90–94.
McEwen, A. et al., 2007. MRO's High Resolution Imaging Science Experiment (HiRISE). J. Geophys. Res. 112, http://dx.doi.org/10.1029/2005JE002605.
McEwen, A. et al., 2010. The High Resolution Imaging Science Experiment (HiRISE) during MRO's Primary Science Phase (PSP). Icarus 205, 2–37.
Möhlmann, D.T.F., 2008. The influence of van der Waals forces on the state of water in the shallow subsurface of Mars. Icarus 195, 131–139.
Möhlmann, D., Thomsen, K., 2011. Properties of cryobrines on Mars. Icarus 212, 123–130.
Paige, D.A., Bachman, J.E., Keegan, K.D., 1994. Thermal and albedo mapping of the polar regions of Mars using Viking thermal mapper observations, 1, north polar region. J. Geophys. Res. 99, 25959–25992.
Pilorget, C., Forget, F., Millour, E., Vincendon, M., Madeleine, J.B., 2011. Dark spots and cold jets in the polar regions of Mars: New clues from a thermal model of surface CO_2 ice. Icarus 213, 131–149.
Piqueux, S., Christensen, P.R., 2008. North and south sub-ice gas flow and venting of the seasonal caps of Mars: A major geomorphological agent. J. Geophys. Res. 113, E06005. http://dx.doi.org/10.1029/2007JE003009.
Piqueux, S., Byrne, S., Richardson, M., 2003. The sublimation of Mars' southern seasonal CO_2 ice cap and the formation of spiders. J. Geophys. Res. 108 (E8), 3-1.
Pommerol, A. et al., 2011. Evolution of south seasonal cap during martian spring: Insights from high-resolution observations by HiRISE and CRISM on Mars Reconnaissance Orbiter. J. Geophys. Res. 116, E08007. http://dx.doi.org/10.1029/2010JE003790.
Portyankina, G., Markiewicz, W.J., Hansen, C.J., Thomas, N., 2010. HiRISE observations of gas sublimation-driven activity in Mars' southern polar regions: III. Models of processes involving translucent ice. Icarus 205, 311–320.
Portyankina, G., Pommerol, A., Aye, K.-M., Hansen, C.J., Thomas, N., 2011. Polygonal cracks in the seasonal semi-translucent CO_2 ice layer in martian polar areas. J. Geophys. Res. 117, E02006.
Pommerol, A. et al., 2013. Observations of the northern seasonal polar cap on Mars III: CRISM/HiRISE observations of spring sublimation. Icarus. 225, 911–922.
Portyankina, G. et al., 2013. Observations of the northern seasonal polar cap on Mars II: HiRISE photometric analysis of evolution of northern polar dunes in spring. Icarus. 225, 898–910.
Putzig, N.E., Mellon, M.T., Herkenhoff, K.E., Phillips, R.J., Davis, B.J., Ewer, K.J., 2010. Thermal anomaly in martian north polar erg likely due to near-surface ice. LPI Contribution #1552.
Rivera-Valentin, E.G., Chevrier, V.F., Ulrich, R., Roe, L., 2012. Effects of freezing point depression on martian paleolake stability. Lunar Planet. Sci. 42. #1074.
Schorghofer, N., Aharonson, O., 2005. Stability and exchange of subsurface ice on Mars. J. Geophys. Res. 110, E05003.
Smith, D.E., Zuber, M.T., Neumann, G.A., 2001. Seasonal variations of snow depth on Mars. Science 294, 2141–2146.
Tanaka, K.L., Hayward, R.K., 2008. Mars-north circumpolar dunes: Distribution, sources, and migration history. LPI Dunes Workshop. Abstract #7012.
Thomas, N., Hansen, C.J., Portyankina, G., Russell, P.S., 2010. HiRISE observations of gas sublimation-driven activity in Mars' southern polar regions: II. Surficial deposits and their origins. Icarus 205, 296–310.
Thomas, N., Portyankina, G., Hansen, C.J., Pommerol, A., 2011a. HiRISE observations of gas sublimation-driven activity in Mars' southern polar regions: IV. Fluid dynamics models of CO_2 jets. Icarus 212, 66–85.
Thomas, N., Portyankina, G., Hansen, C.J., Pommerol, A., 2011b. Sub-surface CO_2 gas flow in Mars' polar regions: Gas transport under constant production rate conditions. Geophys. Res. Lett. 38 (8), CiteID L08203.
Titus, T.N., Kieffer, H.H., Mullins, K.F., Chrisensen, P.R., 2001. TES premapping data: Slab ice and snow flurries in the martian north polar night. J. Geophys. Res. 106, 23181–23196.
Titus T., Kieffer, H.H., Langevin, Y., Murchie, S., Seelos, F., Vincendon, M., 2007. Bright fans in Mars' cryptic region caused by adiabatic cooling of CO_2 gas jets. AGU FM. Abstract #P24A-05.
Tsoar, H., Greeley, R., Peterfreund, A.R., 1979. Mars: The north polar sand sea and related wind patterns. J. Geophys. Res. 84, 8167–8180.
Wagstaff, K.L., Titus, T.N., Ivanov, A.B., Castano, R., Bandfield, J.L., 2008. Observations of the north polar water ice annulus on Mars using THEMIS and TES. Planet. Space Sci. 56, 256–265.
Ward, A.W., Doyle, K.B., 1983. Speculation on martian north polar wind circulation and the resultant orientations of polar sand dunes. Icarus 55, 420–431.